INDIVIDUAL TREE CROWN DELINEATION USING MULTISPECTRAL LIDAR DATA

Faizaan Naveed

A Thesis Submitted to the Faculty of Graduate Studies in Partial Fulfilment of the Requirements for the Degree of Master of Science

Graduate Program in Earth and Space Science
York University
Toronto, Ontario, Canada
May, 2019

© Faizaan Naveed, 2019

ABSTRACT

In this study, an improved treetop detection and region based segmentation algorithm was developed to delineate Individual Tree Crowns (ITCs) using multispectral Light Detection and Ranging (LiDAR) data. The dataset used for this research was acquired from Teledyne Optech's Titan LiDAR sensor which was operated at three wavelengths: 1550 nm, 1064 nm, and 532 nm. Using multi-scale analysis the predominant crown sizes in the scene were initially identified and the treetops were detected for small, medium and large tree crowns. An advanced Gaussian based merging strategy, was employed to merge the treetops at different scales to determine the final crown positions. With the improved region growing segmentation method, neutrosophic logic was extensively used to incorporate contextual intensity information in the region merging decision heuristics. The LiDAR positional data was uniquely exploited, in this research, to generate refine crown boundary approximations. The results from the proposed method were compared with manually delineated ITCs to highlight the performance improvements. A 12% increase in the accuracy was observed with the proposed method over the popular Marker Controlled Watershed segmentation technique.

DEDICATION

To my parents, with affection.

ACKNOWLEDGEMENTS

I have benefited immensely from working with my supervisor Dr. Baoxin Hu in the Department of Earth and Space Science at York University. Her tireless work ethic and excellent insight in the field of Computer Vision and Image Processing enabled me to pursue my research in object segmentation and detection.

I would also like to extend my gratitude to Dr. Jian-Guo Wang, Dr. Brent Hall, Dr. Gunho Sohn, Dr. Costas Armenakis and Dr. Aijun An for their mentorship and constructive criticism of my work throughout graduate school. Their professionalism and guidance enabled me to gain a better understanding on my research area.

Financial support for my research was provided by various sources including the Department of Earth and Space Science, ESRI Canada, and Natural Sciences and Engineering Research Council (NSERC) of Canada. I am also grateful to Teledyne Optech for providing me with the Titan LiDAR dataset to carry out my research endeavours. Lastly, I would like to extend my gratitude to ESRI Canada for engaging me on the Emerald Ash Borer project and providing an opportunity to collaborate with the industry.

My learning experience in graduate school would have been incomplete without the support of my lab colleagues and friends. Their constant moral support and advice allowed me to realize my full research potential. I would like to thank Wen Zhang and Dr. Shu Zhang for their programming advice, algorithm improvements and thesis recommendations.

Finally, I would like to thank my mother (Ayesha Siddiqua) and father (Naveed Hamayun) for their moral support and encouragement. My research endeavours would not have been possible without their love, support and understanding.

Table of Contents

List of Tables

List of Figures

CHAPTER 1

INTRODUCTION

Individual tree analysis serves as a foundation in forestry, environmental protection and power line management applications. Analysis pertaining to individual tree crowns (ITCs) critically relies on the accurate delineation and detection of these tree crowns. The delineated ITCs are used for estimating the sizes, ages and heights of tree crowns (Kwak, et. al., 2007; Pouliot, et. al., 2002; Li et. al, 2012), tree species classification (Gougeon, et. al., 2006; Leckie, et. al., 2003) and tree growth monitoring (Yu, et. al., 2004). For the past few decades, many studies have been conducted for ITC delineation using high spatial resolution imagery. Among the popular delineation methods are edge detection (Koch et al., 2006; Pouliot et al., 2005), region growing (Erikson, 2004; Li et al., 2015) and watershed segmentation (Chen et al., 2006; Jing et al., 2012). Even though satisfactory results are obtained from these methods, incomplete crown edges are often detected due to illumination variation within the tree crown. Furthermore, high commission errors are commonly observed in dense tree stands due to the minimal variation in reflectance between two neighbouring crowns.

Recently, with wide availability of Light Detection and Ranging (LiDAR) data, many studies are being conducted to re-examine region-based and watershed segmentation

algorithms for ITC delineation by exploiting the structural differences, canopy boundaries and spaces between crowns exhibited in the LiDAR data. LiDAR point clouds are often rasterized to generate Canopy Height Models (CHMs) where the local maxima represent treetops and neighbouring pixels with lower elevations represent canopies. Even though detailed crown profiles exhibited in LiDAR data allow accurate ITC delineation in open forests (as with passive optical imagery), problems remain in deciduous or mixed forest stands (Hu et al., 2014). In deciduous or mixed forest stands, tree crowns have varied sizes and overlaps among different crowns forms tree clusters without discernible structural parameters for ITC delineation.

Studies have also indicated that the structural information from LiDAR data is useful in the identification of trees, but the spectral information in optical imagery remains a better source for discerning the boundary between adjacent crowns (Zhen et al., 2016; Briedenbach et al., 2010). As a result, the structural and spectral differences between tree crowns exhibited in LiDAR data and passive optical imagery, respectively, are incorporated in several studies to improve ITC delineation. With most of the methods, the CHM derived from LiDAR data is utilized to identify treetops, and the reflectance from optical imagery is used in the delineation of the crown boundaries using seeded region growing (SRG) or maker-controlled watershed (MCW) segmentation (with the detected treetops as the initial seeds or markers, respectively (Briedenbach et al., 2010; Zhen et al., 2016). A very limited number of studies have examined the benefits of integrating LiDAR data with optical imagery at the crown delineation phase (Zhen et al., 2016). Lee et al., (2017) proposed an integration strategy to generate graph weights using both optical image

and LiDAR data in a graph cut approach. Their method was tested on coniferous stands and the reported accuracy metrics (ratio of extracted trees to the matched trees) were around 50%. Lee et al (2017) further stated that around 100 LiDAR pixels were represented by a single hyperspectral pixel, which made it difficult to analyse the benefit of integrating spectral and structural information in ITC delineation (Lee et al., 2017). Apart from the large differences in the spatial resolution between the two datasets, issues and uncertainties in their co-registration also posed problems (Lee et al., 2017).

As illustrated in Lee et al., (2017), the successful integration of LiDAR and optical imagery critically relies on the spatial resolution, coverage and minimal relief in the optical imagery. These requirements are difficult to obtain particularly if the datasets being integrated are collected from different missions at different times with different configurations (i.e. flying height, view angle, scan direction et cetera). Despite rectifying these differences, problems still exist due to shadows and registration errors (Lee et al., 2017). Current advances in the multispectral LiDAR technology provide a good opportunity to improve ITC delineation using spectral and structural information without encountering the frequent problems present in the integration of datasets from different missions and configurations. Multispectral LiDAR provides 3D coordinates of surface objects and the reflected intensities of the target by simultaneously emitting pulses and collecting returns at different electromagnetic wavelengths. The multispectral Titan LiDAR instrument of Teledyne Optech (www.teledyneoptech.com) is an airborne sensor that collects three different point clouds together with corresponding intensities at three wavelengths (1550 nm, 1064 nm and 532 nm). Since the three point clouds (with 3D coordinates and intensities) are

collected simultaneously with similar point densities (via the same platform), minimal processing is required to co-register the three data clouds. A few of the studies have reported the use of the Titan multispectral LiDAR data for land cover classification purposes (Morsy et al., 2016; Diaz et al., 2016; Zou et al., 2016), but none have investigated their applications in improving ITC delineation.

The goal of this research was to exploit the capabilities of multispectral LiDAR data in the improvement of ITC delineation by fully and effectively utilizing the combined structural and spectral information of tree canopies. With most ITC methods, trees are usually detected first, and segmentation methods, such as seeded region growing, and watershed are then used to delineate the crown boundaries. This study aimed to improve the tree detection phase and the ITC delineation phase by integrating structural and spectral information. To achieve the research goal, the following specific objectives were identified and fulfilled.

1) Develop procedures for pre-processing the Titan multispectral data

Even though the methods are proposed to co-register the data clouds collected at different wavelengths and normalize the returned power for radiometric corrections, a completely integrated framework for pre-processing the Titan multispectral LiDAR data is not present (Yan and Shaker, 2015 & 2017). Furthermore, most methods are focused on improving the quality of the spectral information but do not emphasize on approaches for processing the LiDAR positional (i.e. structural information). In this study, a complete work flow to

radiometrically correct and co-register the multispectral Titan data was proposed and implemented. The intensity data was radiometrically corrected to remove the effect of ranges on the received target intensity. Processing to remove the effect of incidence angle, using a cosine correction, was not performed, as it induced over-correction in certain scenarios (Yan and Shaker, 2014). The LiDAR positional information was processed to extract the true dimensions of the canopy by eliminating the underlying low-frequency positional trend. Using a reference channel, determined by the maximum penetration power of the EM wavelength of the emitted pulse, a grid was formed, and the data co-registered via Inverse Distance Weighted (IDW) interpolation. The grid size was determined using the average returns per square meter in the three data clouds. The interpolation was then performed using the largest possible grid size to prevent gaps in resolution between the different intensity bands. Moreover, to mitigate the effect of scan lines, a smoothing kernel proportional to the crown size, was homogeneously applied over the interpolated intensity channels and the positional data. The integration strategy presented a simple yet effective framework for multi-wavelength LiDAR data. Further details on the integration methodology are outlined in the data pre-processing section.

2) Improve multi-scale analysis for treetop detection by developing an advanced integration strategy for merging treetops identified at different scales

Treetop detection methods (Zhang et al., 2015; Wang et al., 2004) rely on local maximum filtering (LMF) techniques to identify the local maxima as the treetops in the scene. However, with varying crown sizes, such methods yield high commission errors due to the

false detection of treetops. Since trees, particularly in natural forest stands, tend to have varying sizes, multi-scale approaches are increasingly preferred (Jing et al, 2012 and Hu et al, 2014). Among the existing methods in the detection of treetops, the method proposed by Jing et al, (2012) and Hu et al (2014) had significant advantages over others as it accounted for varying crown sizes in the scene. Additionally, instead of detecting treetops as individual pixels, like most of the treetop detection methods, the multi-scale method detected the largest horizontal cross-sections of the tree crowns, which were not sensitive to noise in the data. However, Jing et al., (2012) and Hu et al., (2014) only proposed a simplified approach to merge the treetops at different scales based on a measure of region circularity. As a result, the method was sensitive to the initial selection of appropriate scales (to reflect the dominant crown sizes in the scene), which were difficult to detect (Hu et al., 2014). To rectify these issues, an advanced merging strategy was proposed to integrate the identified treetops at different scales using LiDAR shape information.

3) Develop a region-based ITC delineation method to effectively combine the structural and spectral information of tree canopies

Among the existing segmentation methods, region growing has advantages in terms of combining information from different data sources. Region-based methods rely on the assumption that adjacent pixels (belonging to the same object) have similar features based on the grey-level, colour or texture. Using a pre-defined homogeneity criterion, region-based methods merge adjacent pixels with similar features to produce a segmentation map. By exploiting high level knowledge of the image, seeds can be initialized to provide initial

approximations of the objects in the image. Since region-based methods do not make any morphological assumptions about the image, it is relatively easier to integrate different data sources by modifying the homogeneity criteria, statistics and imposing shape, size and texture based constraints on the growing patterns. Different similarity metrics can be constructed that reflect the underlying nature of the object in each data source (i.e. in LiDAR a morphological based similarity measure can describe the structural parameters of the crown whereas in optical imagery, first and second order statistics can be used to describe the spectral signature of the crown). Additionally, each similarity metric, characterizing a unique data source, can be weighted based on a measure of uncertainty to mitigate the effect of noise present in that dataset. Watershed segmentation and edge-based methods, in comparison, do not offer such versatility in integrating different data sources. Due to their dependency of intra-crown illumination variation to detect the edges in the image, watershed and edge-based methods tend to be sensitive to noise. Furthermore, it is hard to integrate multiple channels (i.e. data sources) in such methods as they primarily rely on assumed topology in the image. As a result, a region-based method was employed in this study to perform the ITC delineation.

Existing studies that employ region-based ITC delineation methods do not emphasize on data integration at the delineation phase (Zhen et al, 2016; and Hyyppa et al., 2005). Even though several studies have proposed modified region-based ITC delineation methods, few have accounted for their expendability to ITC delineation using multiple data sources. The current region-based ITC delineation methods need to be improved in two aspects: an

integration strategy to merge different data sources and a contextual similarity measure to account for varying levels of noise in the dataset.

To combine spectral and structural information in ITC delineation, studies, in the past, have used the CHM, derived from LiDAR, with optical imagery, in a multi-dimensional segmentation method by appending the CHM as an extra band onto optical imagery (Briendenbach et al., 2010; Zhen et al., 2016). Such approaches fail to fully exploit the crown morphology by treating the CHM has another spectral band with same homogeneity criterion. In this study, the structural information, in the CHM, was used to impose a positional constraint onto the growing regions by accounting for the natural morphology and shape of the crown. The positional constraint was used to eliminate neighbouring pixels of the growing patterns that did not conform to the morphological template of the tree crown, defined via a Gaussian function.

In a second improvement to the region-based segmentation method a new contextual similarity measure based on neutrosophic logic was proposed. Neutrosophic logic was initially used to segment tumours in noisy ultrasound images (Shan et al., 2008). In this study neutrosophic logic was employed, for the first time, to perform ITC delineation. Dependent on a measure of variance, around the pixel of interest, the similarity criterion was adjusted to account for contextual information to prevent the merger of noisier pixels to the growing regions (Naveed and Hu, 2017). The approach also mitigated the effect of outliers in the dataset as the decision heuristics were derived using a weighted average of

multiple pixels. The final metric for intensity was also adjusted to prevent noisier channels from having an equal weightage in the final merging decision.

The proposed modifications, explained in further details in the proceeding sections, were shown to reduce cases of over and under segmentation and reduce omission errors in the generated segmentation map. Combined with the treetop detection phase a complete region-based ITC delineation framework, from multiple data sources, was presented. This study offered insight into ITC delineation from multiple data sources and addressed common cases of over and under segmentation by proposing a neutrosophic region growing method from integrated LiDAR data and spectral information (Naveed and Hu, 2017).

The rest of this thesis is structured as follows: section 2 introduces the background literature for this research. The commonly used architectures for ITC delineation are discussed and analysed. The concept and operations of the LiDAR are also introduced. The study area, dataset and reference tree crowns are introduced in section 3. Section 4, outlines the data pre-processing required prior to the ITC delineation framework. LiDAR intensity and positional data processing are individually discussed in this section. The ITCD framework is presented in detail in section 5: improved multi-scale method and region-based segmentation method, proposed in this study, are described in detail. A quantitative measure of accuracy assessment is also presented. Section 6 outlines the qualitative and quantitative results and provide a critique of the treetop detection and ITC delineation method. The conclusion and further improvements are suggested in section 7.

CHAPTER 2

LITERATURE REVIEW

ITC delineation dates to the 1990s when edge-detection methods were popularly applied to aerial and satellite imagery to extract crown boundaries (Gougeon, 1995). Many advanced methods have since been developed that exploit other properties of crowns for ITC delineations. These methods can be roughly broken down into three categories: Edge-based methods, watershed segmentation and region-based methods. Even though different variants of these methods have been applied to different datasets (satellite and aerial imagery and LiDAR datasets), majority of the methods do not work well in dense mixed forest or deciduous stands (Chen et al., 2006; and Li et al., 2012). In the following sections, the LiDAR data including multispectral LiDAR data and different ITC delineation methods are described in detail.

2.1 Multispectral Light Detection and Ranging (LiDAR)

Light Detection and Ranging (LiDAR) instrument is an active remote sensing sensor that collects 3D coordinates of a distant target while moving along specific survey routes. By rapidly emitting discrete laser pulses, the instrument measures the time it takes for the pulse

to interact with the target and return to the sensor. The distance to the target is then computed by considering the travel time between the target and the receiver and the speed of light (Carter et. al., 2012). Combined with Global Position System (GPS) and Inertial Measurement Unit (IMU) data, the distance measurements are transformed to a 3D point cloud of the observed target area. The GPS and IMU provide the coordinates of the LiDAR scanner, and using range and angular measurements the coordinates of the observed target are determined. The results of a LiDAR survey, hence, yield a highly precise geo-referenced point cloud with Easting (*E*) and Northing (*N*) coordinates and the elevation (*U*). In addition to collecting the 3D coordinates of the observed target area, LiDAR instruments also record the return power (i.e. intensity) (Wehr and Lohr 1999 and Baltsavias, 1999).

Laser beam divergence, field-of-view (FOV), sensor altitude and view angle from the nadir control the size of the circular sampled area on the ground, called the footprint. A narrow beam-width can yield a smaller footprint (5-30 cm) and more precise Easting and Northing coordinates. The density of the point cloud is controlled by the pulse rate frequency (PRF), scan speed and platform speed. These days the LiDAR can collect data with spatial grid resolution of < 0.5 meters. The scanning method varies, but the commonly used variant is a bi-directional scanning mechanism that scans line by line producing Z shaped patterns. Since the sensor collects data laterally to the flying direction, the point density tends to be slightly higher at the edges of the point cloud.

Most existing LiDAR instruments operate in one single wavelength. The working wavelength for a topographic LiDAR instrument is often in the near-infrared varying from 1000-1500 nm. Titan multispectral LiDAR (Teledyne Optech Inc., 2014) is the first of its kind that collects data in three spectral channels. This is achieved by installing three different sensors with different spectral wavelengths on board the same airborne platform. The three channels are collected at different viewing angles: 1550 nm at 3.5° forward looking, 1064 nm at 0° nadir looking, and 532 nm at 7° forward looking direction. Even though traditionally LiDAR instruments are known to provide accurate positional information, multispectral LiDAR also offer rich spectral information that can be exploited together the positional information in ITC delineation studies.

Various radiometric correction methods have been developed to process the intensity data from discrete waveform LiDAR using the radar equation (Jutzi and Gross, 2010; Yan and Shaker, 2016). Radiometric correction accounts for system and atmospheric attenuation, ranges and incidence angle to retrieve the at surface reflectance of the target objects. Furthermore, radiometric normalization is also performed to co-register and normalize the intensity data from overlapping LiDAR strips by mapping the LiDAR strips to a selected reference using distance thresholding techniques (Yan and Shaker, 2016). For the Titan LiDAR data, Yan and Shaker (2017) proposed a polynomial approximation to model the laser attenuation as a function of the range and angle loss. The study also reported that the use of cosine correction for incidence angle loss was inefficient for different wavelengths and different land cover types (Yan and Shaker, 2014). In a separate study Yan and Shaker (2016) also examined the co-registration of different LiDAR strips by generating a joint

histogram for radiometric normalization. Using the LiDAR strip with the largest intensity range as reference, the overlapping strips were radiometrically normalized with respect to the reference and interpolated to generate the final intensity bands.

Several studies have exploited the spectral capabilities of the Optech Titan LiDAR in examining cover type classification of 3D point cloud data (Morsy et al., 2016; Diaz et al., 2016; Zou et al., 2016). Zou et al. (2016) examined the benefits of multispectral LiDAR point clouds for 3D land cover classification. The paper reported using an object based classification approach by prior segmentation of the intensity/spectral data and consequently using the segmentation map in a feature level classification. However the segmentation carried out by Zou et al. (2016) was a broad cover type segmentation to classify different cover types (i.e. high vegetation, low vegetation, water, road, building, et cetera). Furthermore no accuracy metrics were quoted for the segmentation results. Morsy et al. (2016) also used the Titan dataset for a land water classification using a region growing method. Using elevation, intensity and geometry based features, initial seed points were selected for the water cover type and region growing was used to discriminate water from land. Though many other studies have been conducted to exploit the benefits of multispectral LiDAR data, few have examined its capabilities in ITC segmentation. Furthermore, studies that have examined the effects of exploiting Titan spectral data for object segmentation have performed a broad cover type segmentation primarily for object classification purposes. In this study we offer an insight into the benefit of multispectral LiDAR data in ITC segmentation by examining the nature and quality of the spectral information and its integration with the structural data.

2.2 Edge-Based Methods

Edge-based methods are among the earliest and popular methods that were used for ITC delineation (Gougeon, 1995). With edge-based approaches, edges are usually generated first by an edge-detection algorithm and then linked to continuous boundaries that outline the resulting segments through post-processing. Most edge-detection method rely on a constant or variable sized operator to detect initial edges (i.e. crown boundaries) in the scene and then incorporate edge linking as a post processing step. However, these types of methods are very sensitive to noise, and tend to over-segment the image easily. A more sophisticated edge-detection method relies on illumination variation between crowns to track pixels of the lowest illumination, representing the crown boundaries (Gougeon, 1995). This category of method, known as valley following approach, was originally proposed by Gougeon (1995) and further refined by Gougeon et al., (2005). It tracked pixels of the lowest illumination in an 8-connected neighbourhood and used thresholding techniques to mask out small areas of shade. The study was tested on IKONOS imagery with a spatial resolution of 4 x 4 meters however the ITC delineation results were not validated to assess the quality of the detected crown boundaries.

2.3 Watershed Segmentation

The watershed method assumes the image to be an inverted topographical surface where the local minima represent the tree tops and the apexes are the crown boundaries (Beucher and Lantuejoul, 1979; Meyer and Beucher, 1990; Vincent and Soille, 1991). There are

different variants of the watershed method, but the original and the most popular variant is Marker Controlled Watershed (MCW). It exploits a flood fill strategy, where starting at the local minima (markers), neighbouring pixels are examined and merged to the respective markers based on the gradient magnitude of the pixel (Jing et al., 2012; Chen et al., 2006; Wang et al., 2004). Unlike region-based methods, described in the following section, no threshold needs to be specified as a pixel is simply added to the marker based on the gradient magnitude of that pixel. Due to the absence of a threshold or constraint, the regions are often over-segmented, generating irregular segments. Furthermore, MCW relies on radiometric peaks in the image to detect the initial markers and the crown boundaries are identified as the lowest radiometric points. This assumption does not always hold true particularly in dense deciduous stands where many non-treetop local maxima and non-crown boundary local minima may be present due to the complex structure of overlapping crowns.

Wang et al., (2004) used a MCW algorithm to delineate ITCs in a 256x256 Compact Airborne Spectrographic Imager (CASI) image of a commercially thinned forest. A two-step process was employed to initially generate an edge map using Laplacian of Gaussian filter, and then applying local maxima filtering to generate tree tops, which were used as markers in the MCW segmentation. It was reported that an average pixel agreement of 75% between manually delineation and MCW results. It was worthy to mention that the study area, in Wang et al., (2004), was a commercially thinned forest that consisted of regularly spaced crowns with large gaps between adjacent crowns (i.e. there was minimal presence of tree clusters in the scene), which was a major factor for the reported high accuracies.

Chen *et. al.* (2004) also used MCW to isolate individual trees in a Savannah woodland using a small footprint LiDAR data. A Canopy Maxima Model (CMM) with a variable window size was proposed to initially detect treetops. The window sizes were determined from a regression curve between the crown size and tree height. Using an adaptable window size, the commission errors were reduced in the detected treetops by eliminating non-tree top local maxima in the CMM. The CMM also provided an ideal surface for watershed segmentation. Chen et. al. (2004) used two instances of segmentation to delineate the ITCs. The initial delineation was used to generate a distance-transformed image and refined tree top markers. A second watershed segmentation was then performed to generate final crown segments. The accuracy of delineation was evaluated using an Absolute Accuracy for Tree Isolation (AATI), which was a measure of the ratio of overlap between the delineated crown segment and reference polygon. An error margin of 10% between the delineated crown and the reference polygon was used for the calculation of the AATI. The reported average cross-validation accuracy was 64.1%. In addition, over-segmentation remained an issue due to the presence of irregularly shaped old oak trees. Furthermore, commission errors also originated from dense tree clusters which were difficult to delineate even with initial markers.

To mitigate the problem of over-segmentation due to the complex upper branch structure of deciduous crowns, Jing et. al. (2012) proposed a multi-scale filtering and segmentation method. Morphological opening operations (Serra et al., 2012) were used to identify the dominant scales corresponding to the sizes of tree crowns within the scene of interest and detect the cross-sections of tree crowns at the identified scales. It was reported that the

morphological opening operations with multi-scale analysis was able to remove the upper branch structure and detect cross sections of the crowns (as compared to the tree tops) at different tree heights. This was reported to greatly reduce the number of falsely identified tree tops. Watershed segmentation was then performed using the identified 'treetops' at different scales. A post segment boundary refinement process was used to combine the segments maps at different scales to produce the final crown segments. The methodology was tested on three plots containing mixed, coniferous and deciduous crowns. The final accuracies reported were 124 crowns matched out of 222 for the plot containing mixed trees, 160 out of 251 matched for the plot containing coniferous trees, and 84 out of 167 matched for the plot containing deciduous crowns. A match was reported as an overlap of greater than 50% between the segments and the manually delineated reference polygons. The reported results were poor particularly for the deciduous and mixed plots due to the complex crown structure. The overlap of branches between deciduous crowns was reported as a large error source, which could not be completely mitigated using multi-scale analysis proposed in the paper.

2.4 Region-Based Methods

Region-based methods rely on some measure of distance or statistical significance to merge pixels to their respective regions. A variant of region-based methods known as Seeded Region Growing (SRG) works on a similar principal to MCW, where the seeds (i.e. treetops) are initially identified and the neighbouring pixels are merged to those seeds based on a similarity metric. The regions are grown until the boundaries of the crowns are

realized. Different similarity metrics have been proposed but the commonly used ones are Euclidean distance (Baartz and Schape, 2000; Li et. al., 2012) and absolute distance (Novotný et al., 2011). Majority of the studies do not account for any contextual information when computing the similarity metric and instead rely on heuristics derived based on single pixel alone. This, as address in the methodology section, is one of the main factors that can contribute to erroneous segmentation.

Li et al., (2012) proposed a region-based ITC segmentation method by exploiting the 3D structure of a small foot-print discrete return LiDAR in a mixed conifer forest in California. A top-down rule-based approach was used to segment the tree crowns starting from the tree tops. The regions were grown by including nearby points based on a distance and height threshold. Points greater than a certain threshold were excluded from the target region and points below the threshold were classified based on a minimum distance rule. To account for adjacent tree crowns, a mutual distance metric was computed to decide the point assignment between the two competing regions. Additional compactness-based rules were incorporated by generating a 2D convex hull of the points in the growing region. The paper reported a recall and precision values of 0.86 and 0.94. The accuracies were significantly high, but the plot used consisted of predominantly coniferous tree crowns which do not exhibit significant overlap with adjacent crowns due to their structure and are relatively easier to delineate (Jing et. al., 2012). As a result, such high accuracies are easier to obtain, particularly with LiDAR data as it offers a detailed vertical profile of the tree capturing the elongated coniferous crown structure.

A more recent paper by Zhen et al., (2015), introduced an agent-based region growing method for ITC delineation using airborne laser scanning data. Unlike previous studies, it was tested on both coniferous and deciduous stands. The paper examined three different methods: MCW with simultaneous growth of all regions (as compared to traditional MCW in which each region is grown fully before the next region is examined), agent-based region growing with one-way competition and agent-based region growing with two-way competition. One-way and two-way competition were used to mimic the natural growth of tree crowns in an ecological environment. This idea was based upon the assumption that competition for sunlight, in a forest, effects the growth and development of tree crowns. Taller trees receive more sunlight then shorter trees in a crowded scene, which in turn affects the growth, crown symmetry, and structure of the trees. One-way competition was used to describe the in-effect of smaller trees on larger trees whereas two-way competition illustrated the effect of smaller trees on larger trees and vice versa. The stand density and the ratio of the average distance between trees and the average height of the canopy were used in one-way and two-way competition in the region growing algorithm. In one-way competition, trees of smaller height could not compete with higher trees whereas in two-way competition smaller trees could affect larger trees and vice versa. Specifically, if two growing regions were competing a smaller tree could take pixels from a larger tree and vice versa in two-way competition, while in one-way competition only the higher tree could take pixels from the smaller tree. The algorithms were tested on four different datasets containing a mixture of coniferous and deciduous plots. The reference data were used to generate initial markers (i.e. treetops) and hence the reported accuracy for tree top detection was 100%. The delineation results were evaluated using the relative error,

measured as the difference in the total area of the delineated and reference crown, and the overall accuracy which considered a greater than 50% overlap between the delineated crown and reference crown as a 1:1 match. It was reported an average overall accuracy of the four datasets were 77.5% and 81.2% for one-way and two-way competition, respectively. The average relative error was reported to be 6.6% and 6.8% for one-way and two-way competitions respectively. The proposed methodology was modelled on an ecological phenomenon to stimulate a natural growing environment for the regions. However, a key component of the region-growing algorithm (the initial tree top detection) was omitted, which allowed the study to assume an ideal scenario: 100% accuracy for tree top detection. In addition, the delineated results were more polygonal in shape than the natural elliptical shape of the crown, despite incorporating several constraints to ensure compact circular regions.

2.5 ITC Delineation Techniques from Multiple Data Sources

There are not many studies that have reported ITC delineation using multiple data sources (i.e. LiDAR data sand optical imagery), despite the potential improvements in discerning crown boundaries in dense deciduous stands (Zhen et al, 2016; and Hyyppa et al., 2005). Briedenbach et al. (2010) reported using a fused airborne laser scanning and multispectral dataset for ITC segmentation and tree species prediction. The LiDAR dataset was collected using the Optech ALTM 3100 EA scanner and the aerial imagery was acquired with Vexcel UltraCam D. The multispectral data contained the Near-Infrared (NIR), Red (R) and Green (G) bands with a pan sharpened resolution of 7500 x 11,500 pixels. The optical data was fused with the airborne LiDAR scan using a rasterized Digital Terrain Model (DTM) based

approach. The DTM was used as an additional channel to the optical imagery, generating a final dataset containing elevation, NIR, R, G channels. The fused data was, consequently, used in a region-based (region growing) segmentation method with constraints on the region shape. It was reported that out of the 2838 delineated ITCs only 52% contained just one tree crown.

Zhen et al. (2013) also reported using a fused LiDAR and orthoimagery dataset for ITC delineation. The LiDAR data were collected from the airborne ALS60 sensor and the orthoimagery was obtained from an open source GIS platform. A rasterized Canopy Maxima Model (CMM) based approach was developed to merge the two datasets. The pit-filled and smoothed CMM was used to register the two datasets using a correlation coefficient by searching for the best match between the CMM and orthoimagery. This was based upon the assumption that the local maxima of heights in the CMM and spectral responses were expected to be similar enough to detect the same trees. The fused datasets were used in a Marker Controlled Region Growing (MCRG) algorithm. The authors did not elaborate on using the fused dataset for crown delineation part but instead investigated the benefits of combining the two sensors in the detection of treetops at both plot and individual tree levels. A Local Maximum Filtering (LMF) treetop detection method was used with a variable window size. The results showed 2%-5% increase in the overall accuracy by using the fused datasets as compared to using LiDAR data alone (~82%). The segmentation accuracy was evaluated by computing the Relative Error of Crown Area (RE_CA) and producer and user Accuracies (PA and UA). A segmented crown was considered a 1:1 match if the overlap between the reference polygon and the delineated

segment was greater than 50%. The authors reported a RE_CA of ~3%, PA of ~60% and UA of ~70%. Despite low segmentation accuracies, the benefits of combining ALS data with the optical imagery for ITC delineation phase were not explored. The prime cause of erroneous delineation was the presence of dense deciduous tree clusters which resulted in multiple regions intersection a single crown (i.e. over segmentation) and certain regions not growing fast enough (i.e. under segmentation).

2.6 Machine Learning Methods for ITC Delineation

Not many studies have examined traditional machine learning based architectures for ITC delineation. Kandare et al. (2014) used a clustering algorithm to segment ITCs in a normalized ALS point cloud. The normalized point cloud was initially divided into slices and k-means clustering was consequently applied to each individual slice. Further cluster merging and splitting was used to eliminate clusters with multi-model distribution as they were deemed to not represent ITCs. The final crown boundaries were then detected as the 2D polygons generated via a convex hull method. Though the method performed well, the total number of delineated trees were often greater than the number of field inventory in both plots. Hence on average the crowns were over-segmented. Zhang et al. (2010) used a Markov-Random Field (MRF) model for individual tree detection from LiDAR data. Local maxima filtering and MRF model was used to detect the treetops and the final crown boundaries were identified using variable crown radiuses. MRF labelling was used to eliminate false treetops based on the location of the top in relation to the boundaries and centre of the crown. A boundary radius constrain was used to penalize local maxima

detected towards the edges of the crown. The final crown boundaries were identified using a variable radius for each identified treetop. Zhang et al. (2010), did not report any accuracy metrics for the results. The visual results indicated a high treetop detection rate, but the tree crowns were not adequately captured by using a constant radius. The plot used in the study was significantly small with a few relatively isolated tree crowns.

Recently deep learning based approaches have become popular for object and instance segmentation. An increasing number of deep learning based architectures have been applied to point clouds as well as optical imagery to segment and/or detect ITCs (Xiao et al., 2018; Li et al., 2016). Majority of these methods rely on a Convolutional Neural Network (CNN) based frameworks to perform instance or semantic segmentation of the image to identify the ITCs. Xiao et al., 2018, used a Fully Convolutional Network (FCN) to detect tree tops from a multi-view high resolution satellite imagery derived DSM and multispectral orthophoto. Instead of generating training data, the study reported using a local maximum detector (top-hat by reconstruction) to find treetops as the pseudo labels. Using a modified variant of the original FCN (Long et al., 2015) with 3 max-pooling layers, the study generated a 2-channel classification probability distribution map that was used to produce the final segmentation map of the treetops. The study reported accuracy metrics of 52.9% in a town area and 88% in the prairie area. Li et al., (2016) used a CNN for oil palm tree detection and counting in a high resolution QuickBird satellite image. The CNN structure (i.e. the number of hidden layers) was optimized via trial and error and the best architecture was then used for final prediction. Using a total of 7200 training images the CNN was trained on 17x17 image patches of oil palm trees and background images. A post

merging step was used to merge false multiple detections based on a distance threshold. The study reported achieving a final testing accuracy of 96% for tree detection with the post merging step. No accuracy metrics were reported for classification output from the CNN directly.

Even though some studies have examined the benefits of applying deep learning architectures for ITC detection and counting, full crown delineation has not been as commonly explored. One of the key setbacks for such studies is the lack of openly available training data for full crown delineation. Additionally the methods work well in regularly spaced or thinned stands, but for dense tree clusters the applicability and accuracy of deep learning methods remains to be explored.

CHAPTER 3

STUDY AREA AND DATASET

3.1 Dataset

The dataset used in this study was acquired by the Teledyne Optech's Titan Multispectral sensor which is operated at three wavelengths: 1550 nm (Channel 1), 1064 nm (Channel 2), and 532 nm (Channel 3). The three channels were collected at different viewing angles: 1550 nm at 3.5° forward looking, 1064 nm at 0° nadir looking, and 532 nm at 7° forward looking direction. The spectral channels had similar configurations with channels 1 and 2 having a beam divergence of 0.35 *mrads* and channel 3 having a 0.7 *mrads* beam divergence. The recommended flying height of the sensor was 300-2000 meters above the ground level (AGL) for topographic applications whereas for bathymetric data collection the preferred flying height was 300-600 meters AGL. The scan angle was programmable between 0 and 60 degrees and the PRF could be configured between 50-300 kHz for each channel. The horizontal accuracy of the point cloud was a function of the altitude (see Table 1) whereas the reported elevation accuracy was 5-10 cm within 1 standard deviation.

Table. 1 Optech Titan LiDAR Data Sheet

Data Specification	
Parameter	**Specification**
Altitude	Topographic: 300-2000 m Above Ground Level (AGL), all channels Bathymetric 300-600 m AGL, C3
Beam Divergence	C1 and C2 ≈ 0.35 *mrad* C3 ≈ 0.7 *mrad*
Point Density	Bathymetric: 15 pts/m^2 Topographic: 45 pts/m^2
Scan Angle	0-60°
Horizontal Accuracy	1σ: 1/7,500 x altitude
Elevation Accuracy	1σ: < 5-10 cm
Pulse Repetition Frequency	50 – 300 kHz (per channel); 900 kHz total

3.2 Study Area

The dataset was collected over the West Rogue, in Scarborough area located South-East of Toronto, Ontario, Canada (Figure 3.1). The scene consisted of a deciduous stand with isolated trees located in urban zones (North-West side of the scene) and dense tree clusters in the woodlot, in the South-East side of the scene in Figure 3.1. The terrain varied in elevation from North-West region representing a flatter terrain to North-East exhibiting higher relief due to presence of a cliff. Due to the absence of field dataset, the exact number of deciduous and coniferous crowns could not be established but an independent examination of Google Earth imagery revealed predominantly deciduous crowns in the scene.

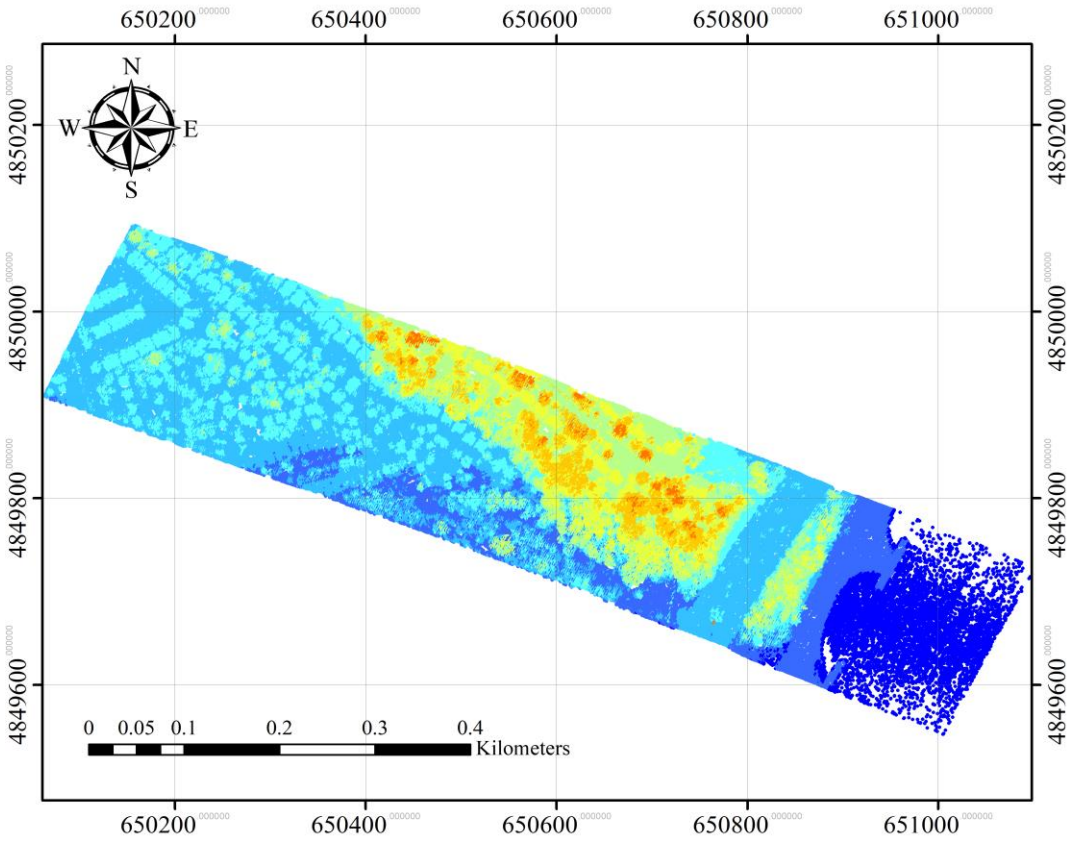

Figure. 3.1. Spatial coverage of the Titan LiDAR scan. The scan was collected over the West Rouge in Scarborough area located southern-east of Toronto, Ontario, Canada.

3.3 Reference Tree Crowns

To validate the results, an independent manual ITC delineation of the scene was performed. To perform the delineation the 3D positional information was utilized along with the spectral data. Prior to performing the manual delineation, the data clouds were radiometrically corrected and co-registered via Inverse Distance Interpolation (IDW) to a common grid (the co-registration and radiometric correction is described in detail in Chapter 4). Each segmented crown was represented by a single polygon in the form of a shapefile. A total of 718 trees were delineated using the spatial toolbox in ArcGIS. The results of the delineation are in Figure 3.2.

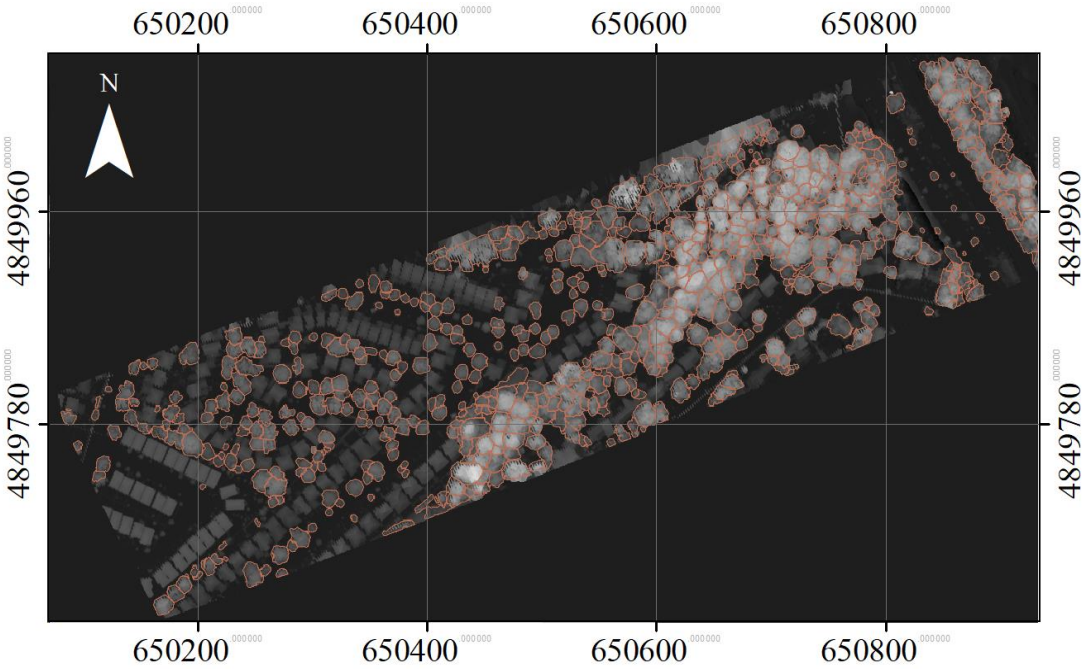

Figure. 3.2. Manually delineated ITCs overlaid on the rasterized Canopy Height Model (CHM). The colour variation from black to white indicates elevation change from low to high elevation, respectively.

Though the spectral and the 3D LiDAR positional data was communally used in manually delineating the ITCs, the positional information was found to be particularly useful in discerning the crown boundaries in the woodlot. The boundaries of the ITCs were considered as the largest cross-section of the tree crown as visualized in the 3D point cloud.

Due to the lack of ground truth information for treetops, the multi scale method could not be quantitatively validated. Reference treetops were generated using the manually delineated polygons. The centroid of each polygon was computed, and a treetop was initialized, at the centroid pixel, using a disk kernel with a radius of 5 pixels. Since the reference tops were computed as the centroid of the reference polygons, they did not represent the local maxima of the tree crowns (i.e. the morphological treetops). Hence the treetops identified with the improved multi-scale method did not align with the reference treetops.

CHAPTER 4

DATA PRE-PROCESSING

The three point clouds in the Titan dataset were co-registered by generating a reference grid. The reference grid was formed using channel 1 (1550 nm). Though channel 1 was used to generate the reference grid, it was observed that the selection of a different channel did not affect the spatial resolution of the grid or the quality of interpolation.

The LiDAR point clouds were interpolated to generate a rasterized CHM and the intensity images corresponding to the three wavelengths of the Titan dataset. To generate the CHM, the Digital Surface Model (DSM) was initially computed via interpolation from the positional information in the 1550 nm point cloud. A Digital Elevation Model (DEM) was subsequently formed to extract the underlying terrain elevation from the DSM to generate the Canopy Height Model (CHM) (CHM = DSM – DEM). The flowchart for the CHM generation is shown in Figure 4.1.

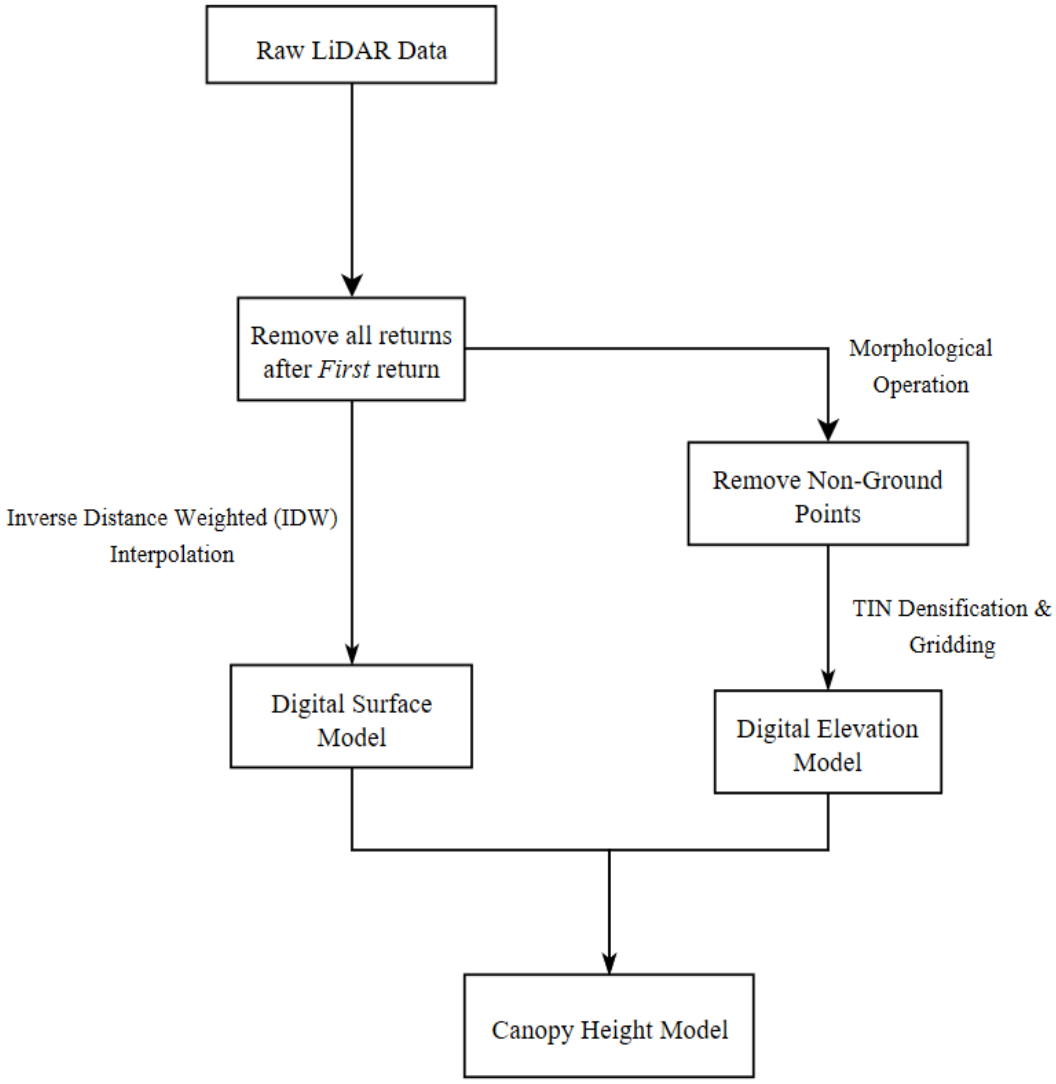

Figure. 4.1. The flowchart of CHM generation. The CHM is generated by subtracting DEM from the DSM.

4.1 Digital Surface Model Generation

To generate the DSM, a reference grid was initially generated using the 1550 nm point cloud due to its higher point density. Due to the different viewing angles and beam divergences there was a systematic shift in the three point clouds. This effect was most noticeable for the 532 nm data cloud, which had the largest difference in viewing angle (7°) from the reference (1550 nm). Despite the differences, it was, however, observed that the selection of reference channel did not significantly affect the spatial extent of the grid as the three point clouds had roughly the same spatial coverage.

To determine the spatial resolution of the grid, the average distance between returns was used (Zhang et al., 2009). This distance was determined by the laser pulse density (first return/m^2) using equation 4.1 (Zhane et al., 2009).

$$d = \sqrt{\frac{1}{\lambda}} \tag{4.1}$$

The average laser pulse density for the first returns was determined to be around 20 returns/m^2 which led to a grid size of 0.25 meters. Using the grid size, the three point clouds were interpolated using an Inverse Distance Weighted (IDW) interpolation algorithm. The choice of interpolation method was again based on the effect of outliers and point density. In comparison with IDW interpolation, kriging was found to perform much worse in interpolating the DSM, due to the presence of non-ground objects. The computed

semi-variogram did not describe the spatial data and the hence the weights for interpolation were not reflective of the underlying spatial auto-correlation in the dataset. Additionally, direct application of kriging to first return LiDAR points resulted in data gaps and fuzzy boundaries (Zhang, 2009). IDW interpolation was, hence, found to be the most optimal interpolation method.

The rasterized DSM is shown in figure 4.2. The DSM had gaps due to the variation in the elevation among the cover types (illustrated in Figure 4.2 c). This was due to the multiple returns being present for each *x, y* location in the grid (hence the most significant gaps were present in tree crowns as multiple returns were predominantly from underneath the tree canopy). To eliminate the gaps, the DSM was generated with only first returns and subsequent returns were removed (illustrated in Figure 4.2 a and b). This was found to remove the gaps and fill the holes in tree canopies.

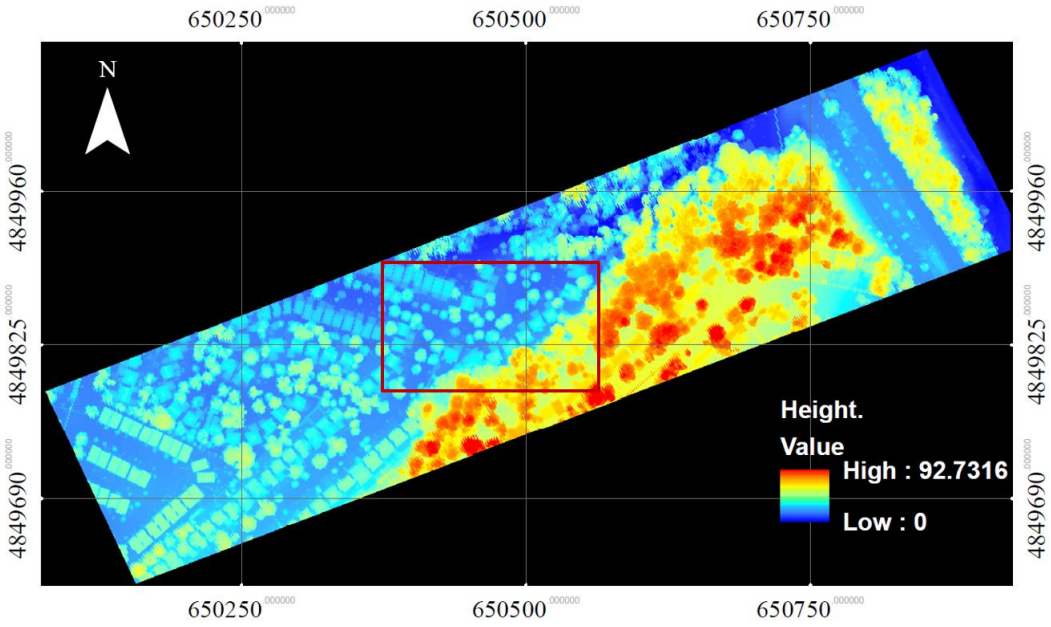

(a)

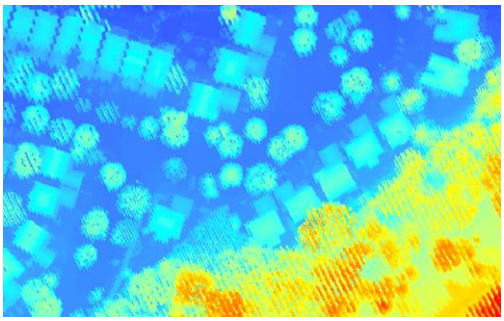

(b)

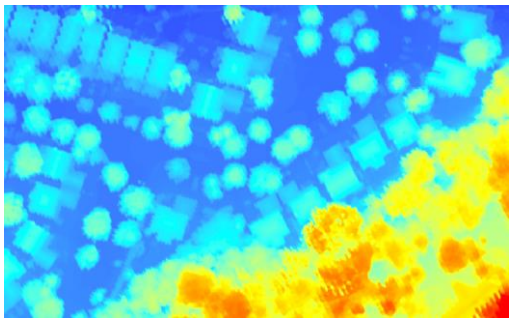

(c)

Figure 4.2. IDW interpolation of the DSM with zoom-in area to illustrate the effect of gridding with multiple returns. (a) The DSM generated via IDW interpolation from first returns with a grid size of 0.25 meters, (b) The zoom-in area of the DSM generated via IDW from all returns with a grid size of 0.25 meters, (c) the zoom-in area of the DSM generated via IDW from first returns with a grid size 0f 0.25 meters.

4.2 Digital Elevation Model Generation

The DEM was generated using an iterative progressive Triangular Irregular Network (TIN) densification (IPTD) method that initially generates a coarse approximation of the ground points and then iteratively refines the approximation by adding more ground points from the original data cloud (Zhao et al., 2016 and Axelsson, 2000). The DEM generation algorithm was implemented in C++ software language with TIN generation capability acquired from the FADE2D library (www.geom.at). The process was divided into two steps: (1) the coarse removal of non-ground points via morphological operations and (2) the refinement of the remaining ground points via TIN densification.

1) Coarse removal of non-ground points via morphological operations

In the first phase of DEM generation, morphological erosion and dilation operations (Serra and Soille, 1994) were used to obtain ground seed points (Zhao et al., 2016). A disk structuring element (SE) was constructed with the radius of the disk reflecting the size of the largest non-ground object in the image. The disk kernel was then used to remove the objects in the point cloud that were smaller than the radius of the kernel using a morphological erosion operation. A disk with a radius of 28 pixels was determined to be optimal in removing all non-ground objects in the dataset. The erosion operation resulted in removal of the ground points (as well as non-ground points) that were smaller than size of the kernel and hence a morphological dilation operation was used to fill the data gaps in the eroded image. By comparing the morphological dilated image with the original point

cloud, the ground points were extracted via a height threshold. A height threshold of 0.65 meters was found to extract majority of the ground points and ignore the non-ground objects in the original point cloud. When selecting the height threshold, a smaller threshold was preferred that could potentially exclude some of the ground points. This approach was used to minimize the presence of any non-ground points, as they could represent inaccurate artefacts in the DEM that could not be corrected at a later stage. The over-erosion of ground data was rectified by an iterative TIN densification process in phase 2.

2) Refinement of the ground-points via TIN densification

In the second phase of the DEM generation, a TIN was generated using a 2.5D Delaunay Triangulation (Lee et al., 1980) algorithm from approximation of ground points from phase 1 (Zhao et al., 1980). The initial approximation of the TIN model was improved by examining the raw LiDAR point cloud and iteratively adding ground points to the TIN. The criterion for determining a ground point was based upon the normal distance from the point to the surface of the TIN and the angle between the three vertices of the TIN and the point (Axelsson, 2000). If the point was determined to be a ground point, then it was added to the TIN and the TIN was reformed. The process was iteratively repeated until all the points in the raw LiDAR point cloud were exhausted. The DEM generation process (Phase I and II) is captured in the flowchart in Figure 4.3.

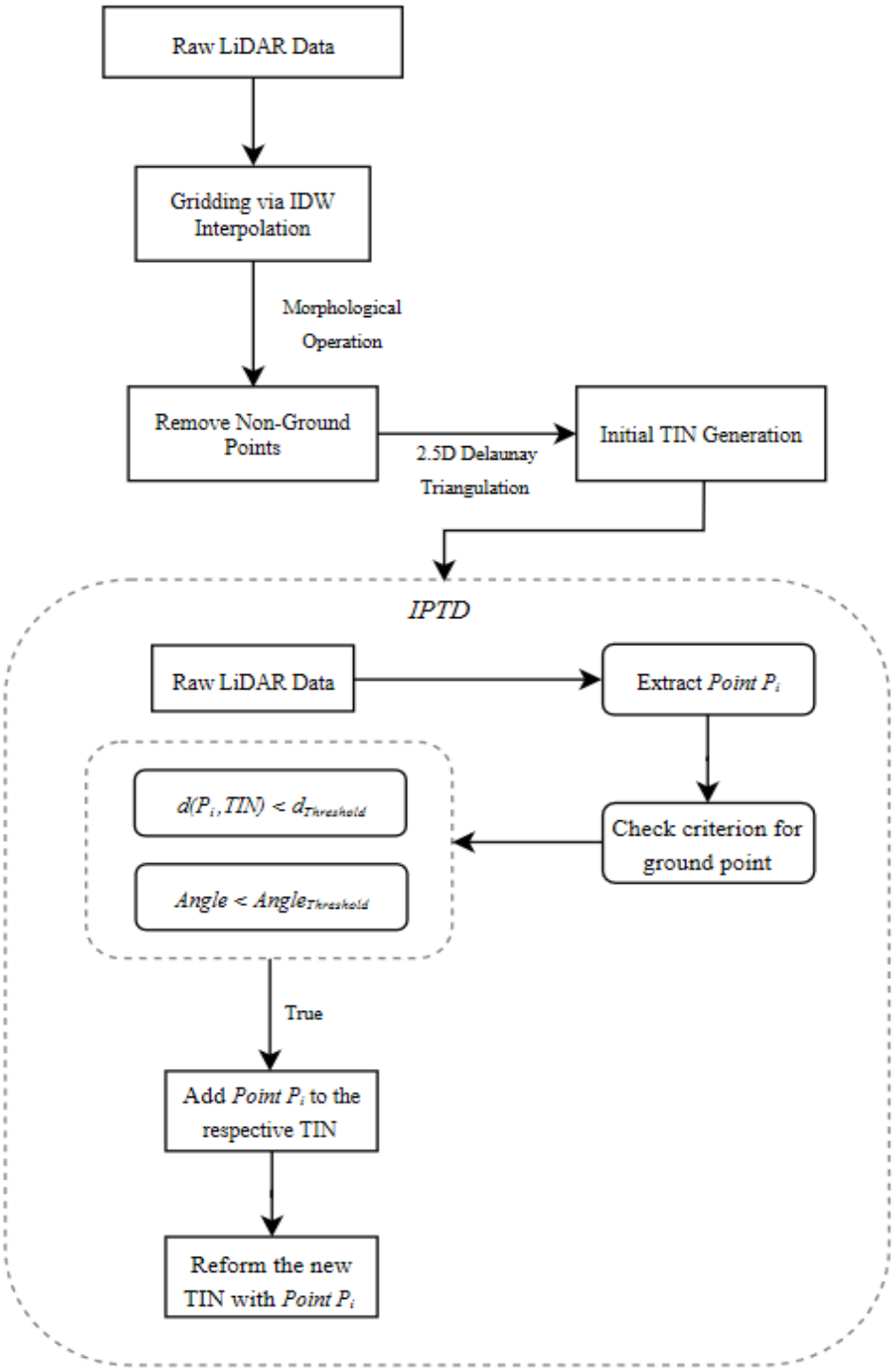

Figure. 4.3. Iterative Progressive TIN Densification (IPTD) for DEM Generation.

Although the first step is sufficient in removing majority of the non-ground points in the point cloud, it inevitably leads to over erosion of the ground data. Due to erosion of the ground data the interpolation can be inaccurate and hence densification of ground points is required to fill the gaps in the data prior to the interpolation. This was found to improve the results, shown in Figure 4.4, in areas of high relief where the terrain was removed due to the large size of the disk kernel.

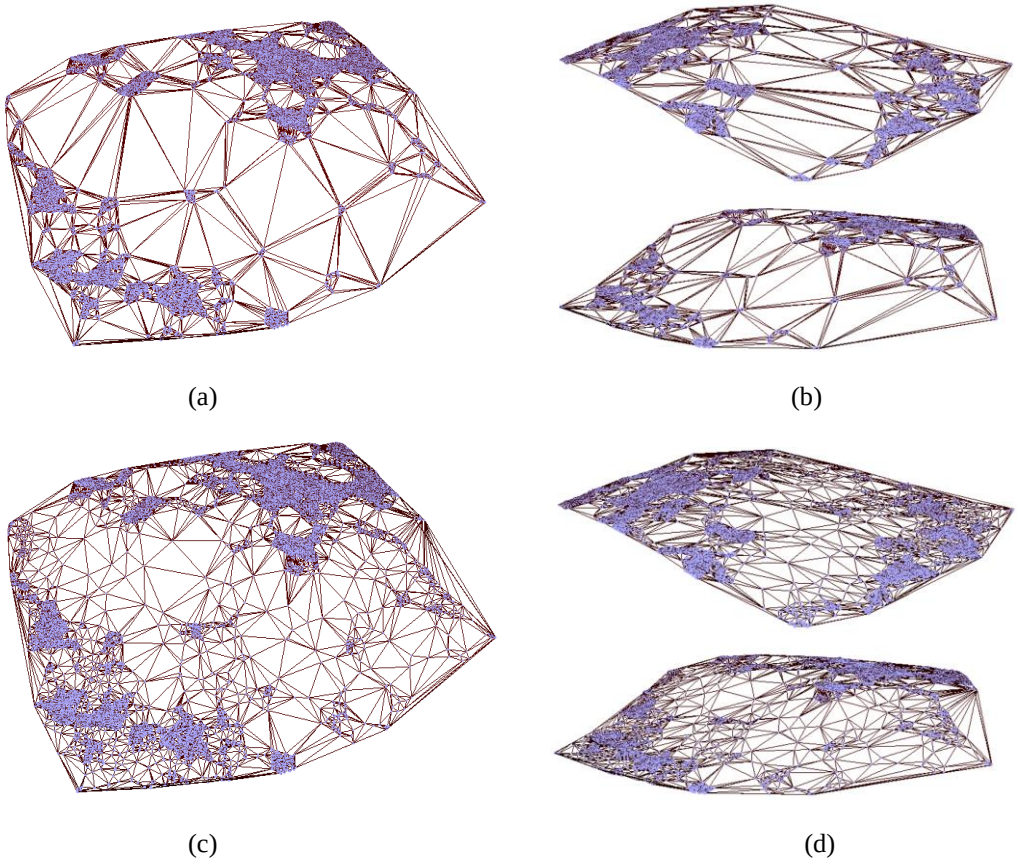

Figure. 4.4. (a, b) Initial TIN model generated from coarse approximation of the ground points in part of the original dataset. Different orientations are presented to visualize the relief in the terrain. (c, d) Post densification TIN model. The slope in the terrain is more defined with the presence of higher number of ground points.

The ground points were used to generate the DEM via interpolation. Different interpolation methods were examined and Inverse Distance Weighting (IDW) was found to be the optimal interpolation method due to its ability to handle inconsistent point density. The same grid size (i.e. spatial resolution of 0.25 *m*) as the DSM was used for interpolation and the results are shown in Figure 4.5.

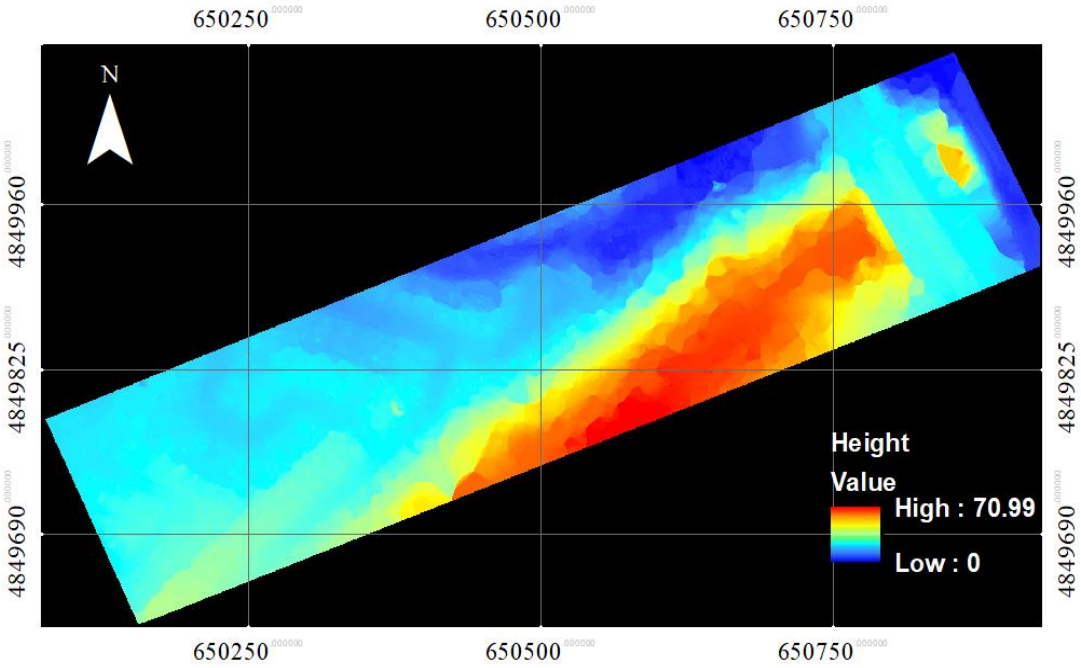

Figure 4.5. The RGB colour coded DEM generated from the Titan LiDAR data over West Rouge, Scarborough, Toronto. The colour code from blue to red represents the change in elevation from low to high, respectively.

4.3 Canopy Height Model Generation

The CHM was generated by subtracting the DEM from the DSM (Figure 4.6). The generated CHM had ‘peaks’ along the edges of the image. These ‘peaks’ were due to the local variation in height within the tree crown (Zhang, 2008). A smoothing operation was used to remove the ‘peaks’ within the crown by applying a Gaussian function. The Gaussian filter was generated by using a kernel size proportional to the average crown size in the scene. A 13 x 13 Gaussian kernel was applied with a standard deviation of 2.5 in the *x* and *y* directions.

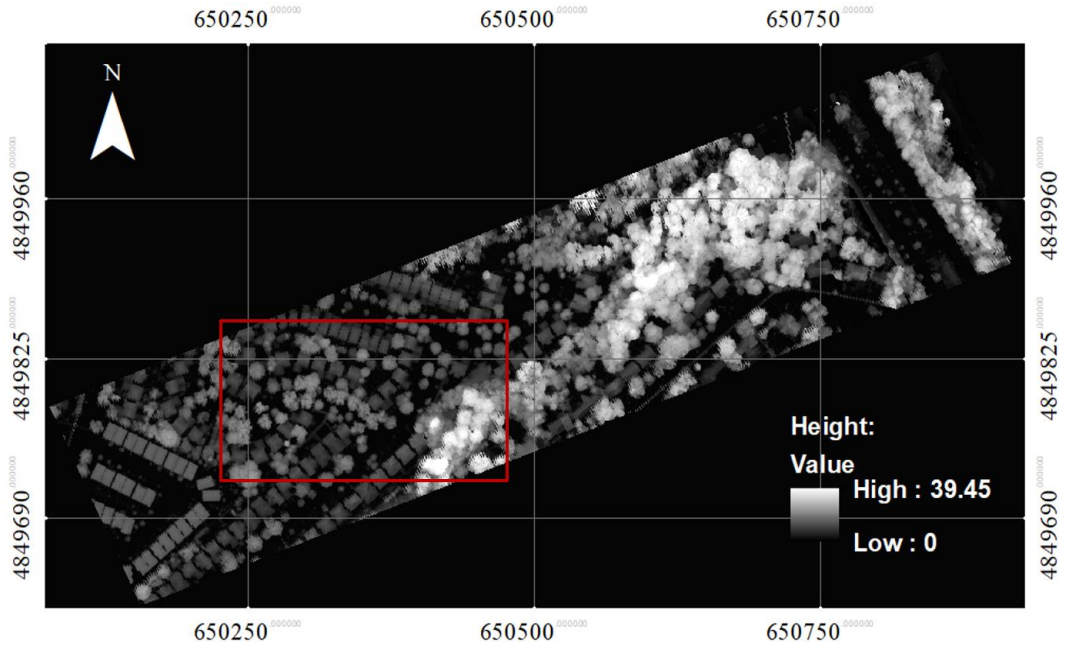

(a)

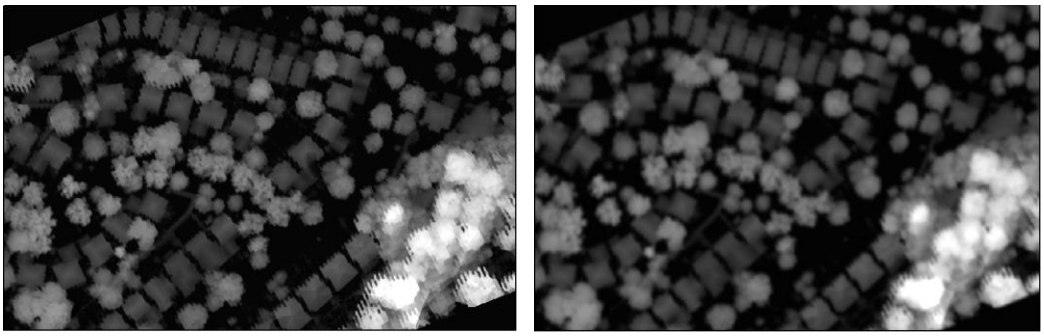

(b) (c)

Figure 4.6. Canopy Height Model. (a) The original CHM generated by subtracting the DSM from the DEM, (b) The zoomed-in area illustrates local variation in height among tree crowns, (c) the zoomed-in area of the smoothened CHM illustrates the mitigation of these local variations in elevation by applying a Gaussian kernel.

4.4 Intensity Normalization

In this study, the intensity information was normalized to remove the effect of ranges. Since the scan angle was not available, correction for the angular loss could not be applied. The ranges were obtained by differencing the target coordinates from the coordinates of the laser scanner (determined via differential positioning using GPS and ground control stations). The intensity data were normalized to remove the effect of ranges from the spectral intensity using equations 4.2 and 4.3. The corrected intensity data is illustrated in Figure 4.7.

$$R = \sqrt{[(E_F - E_G)^2 + (N_F - N_G)^2] + (H - h)^2} \tag{4.2}$$

where E_F, N_F = The coordinates of the laser scanner

E_G, N_G = The coordinates of a LiDAR point

H = Flying height

h = Elevation of the LiDAR point

$$I_c = I * (\frac{R^2}{R_{Max}^2}) \tag{4.3}$$

where I_c = Normalized intensity

I = Original intensity

R_{Max} = The maximal range

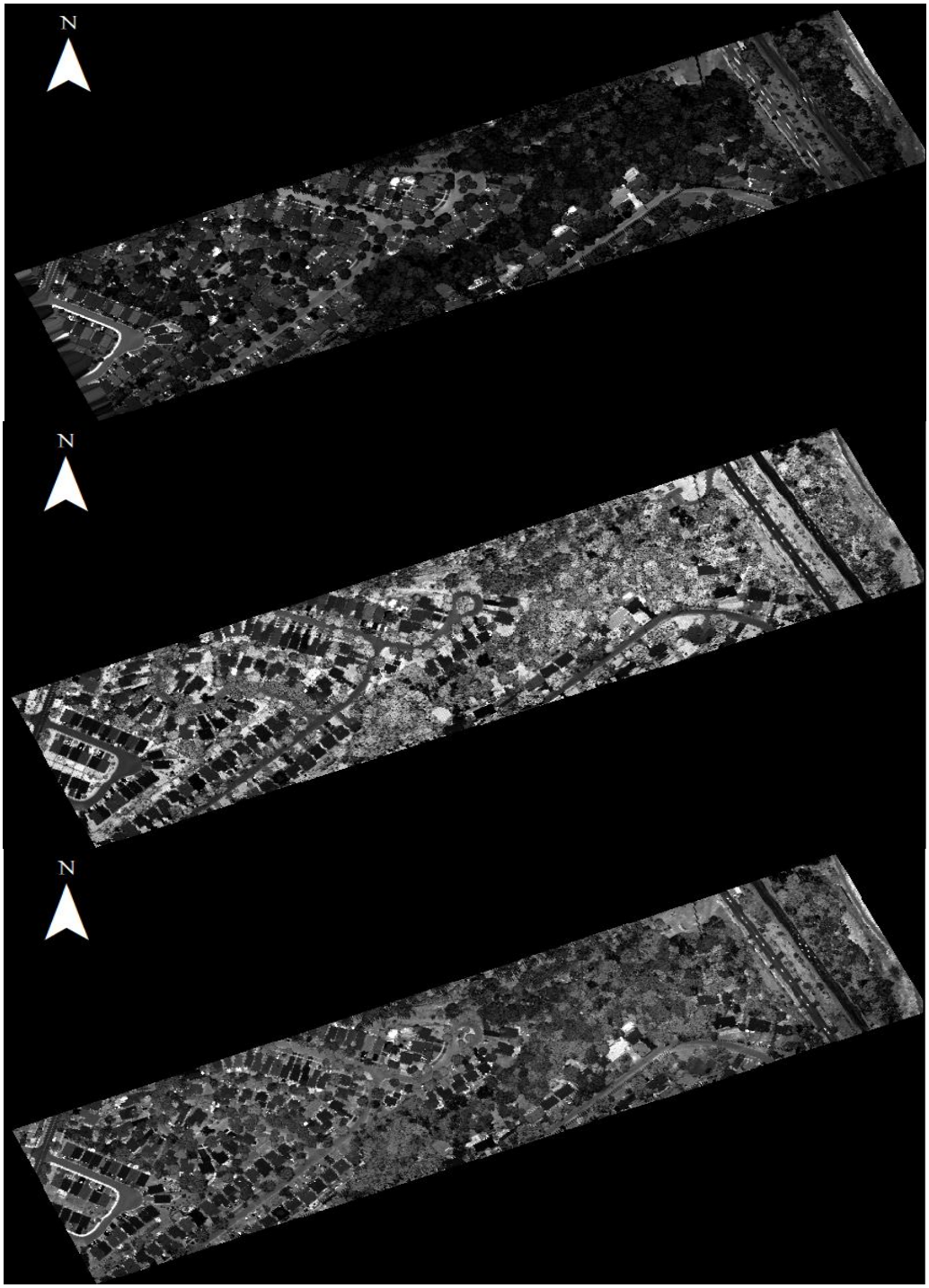

Figure 4.7. Range normalized intensity data (Top panel: 532 nm, Middle panel: 1064 nm, Bottom panel: 1550 nm).

CHAPTER 5

METHODOLOGY

The normalized intensity data and the CHM were used to initially generate a tree mask. An improved multi-scale method was used to detect treetops for varying crown sizes to initialize the seeds for the region-based segmentation algorithm proposed in this study. This chapter outlines the improved architectures for treetop detection and crown boundary segmentation.

5.1 Tree Mask Generation

The normalized intensity and the CHM were used to generate a non-tree pixel mask to remove all non-tree pixels from further processing and analysis. The normalized differenced vegetation index (NDVI) was used to separate vegetated and non-vegetated pixels. The NDVI was calculated using channels 2 and 3 (1064 nm and 532 nm, respectively) using equation 5.1.

$$NDVI = \frac{I_{1064} - I_{532}}{I_{1064} + I_{532}} \tag{5.1}$$

To separate tree and non-tree pixels, a height threshold was defined. Any pixel below the height threshold in the CHM was labelled as a non-tree pixel and replaced by the mask.

A pixel was labelled as a non-tree pixel if the NDVI value was below a threshold of 0.25 and the elevation in the CHM was below a threshold of 4 meters. The mask image was further smoothened via a morphological dilation operation with a disk SE with a diameter of 9 pixels.

5.2 Multiscale Treetop Detection

In this study, an existing multi-scale treetop detection method was improved to mitigate the false detection of treetops. Hu et al. (2014) previously developed a multi-scale treetop detection method to account for different crown sizes in the scene. Instead of detecting single points for treetops, as most of ITC methods, the multiscale approach detected the largest horizontal cross sections of individual trees. In the multi-scale method, the 3D cross-section of a crown, from a near-nadir view, was visualized as half an ellipsoid (Hu et al., 2014). Any single cross section of the ellipsoid was then viewed as a disk with a certain radius identifying the width of the crown at that elevation. A morphological opening operation with disk structuring element (SE) was proposed to remove objects (i.e. upper crown branches) smaller than the size of the specified kernel. The shapes and sizes of the SEs were selected to reflect the predominant crown sizes in the scene. The maxima in a given opened image than represented the cross-section of the tree crown at the corresponding scale.

The scene was processed at multiple scales corresponding to small, medium and large crown sizes and the identified treetops were merged together based on a set of pre-determined rules (Hu et al., 2014). A simple logical OR operation was used merge the

treetops at different scales. The final merged treetops were then used in MCW segmentation to determine final crown boundaries.

Even though the previously developed multi-scale method yielded satisfactory results, issues remained with respect to merging of the treetops identified at different scales. The treetops identified at different scales were merged irrespective of whether the treetop represented the local maxima of the crown or a false local maxima corresponding to upper branches of large deciduous crowns. Furthermore at upper scales, treetops corresponding to smaller crowns were falsely merged into a single treetop which contributed to a high omission error in the final ITC delineation results. Even though a circularity threshold was used to eliminate erroneous treetop detections, there was no indication to suggest that a treetop could not be represented by a non-circular geometric primitive. Hence some treetops representing the local maxima of the crown were also falsely eliminated based on the circularity threshold.

To overcome these problems, a new merging strategy was proposed to combine treetops at different scales during the treetop identification process. Instead of relying on the circularity of the crowns to eliminate erroneous detections, the proposed method used the detailed morphology of the tree crown in the CHM to eliminate treetops that could not be modelled by a 2-D Gaussian function. In this study, a two-step process was used to identify the treetops: 1) the range of scales corresponding to the predominant crown sizes in the scene was initially identified using the mean value analysis of the morphologically opened CHM images; and 2) treetops were identified at these scales and merged based on Gaussian

fitting by initially merging low scale treetops with medium scale treetops and then merging the resulting treetops with large scale treetops.

In step 1, the scales corresponding to the predominant crown sizes in the scene were identified. The scales were selected by analysing the mean of the differenced morphologically opened CHM images (Jing et al., 2012). A series of disk SEs with diameters (i.e. scales) from 3 to 73 pixels, with increments of 2 pixels, were used to generate the morphologically opened images. The opening operation removed the objects with sizes smaller than the SE. As a result, opening operations with a series of different sized SEs were used to determine the dominant crown sizes in the scene. As illustrated in Figure 5.1, the scene with two crowns of different sizes (Figure 5.1 a and d) was processed using two disk SEs of dimeter of 7 pixels (b) and 9 pixels (e). Two tree crowns were retained in the opened image corresponding to the SE with the diameter of 7 pixels (c), since both tree crowns in (a) were bigger than the size of the SE. However, in the opened image corresponding to the SE with a diameter of 9 pixels (f), only the bigger tree crown was retained, as its size was larger than the SE. By comparing the opened images at adjacent scales, the dominant sizes of tree crowns could be identified. In this study, the morphologically opened images at two adjacent scales were differenced and the average of the differenced image was computed and plotted against the scale values. A significant difference in the sizes of the tree crowns between two adjacent scales was then highlighted by a local minima in the plot. The scales corresponding to the local minima in the plot represented the predominant crown sizes in the scene and hence were selected as the final scales for detecting small, medium and large crowns in the scene (Jing et al., 2012).

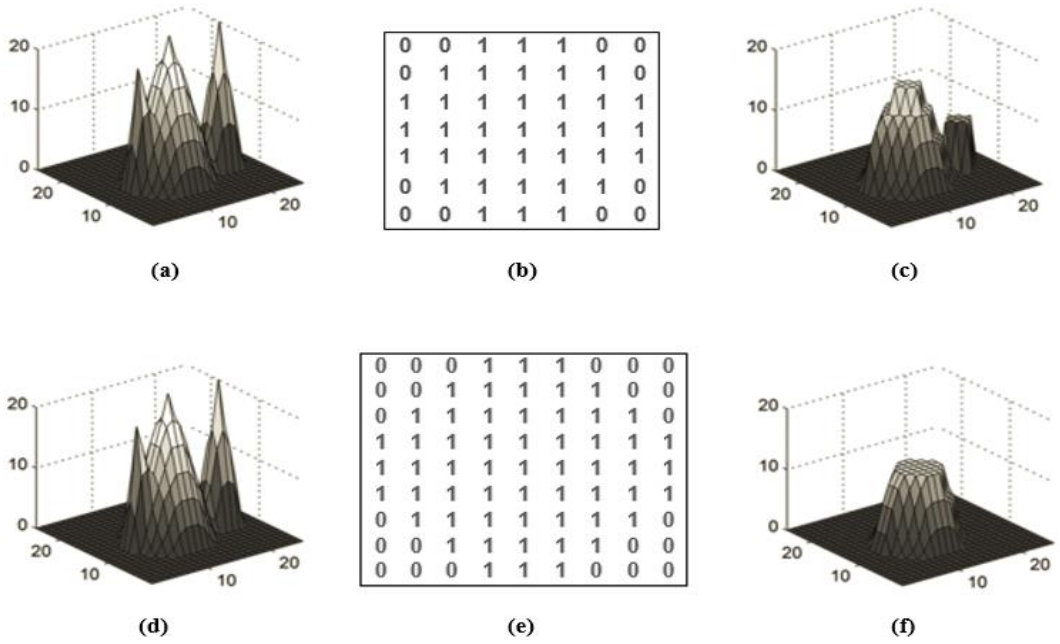

Figure 5.1. Multiscale method visualized as detecting different cross-sections of the tree crown. (a, d) The original 3D representation of the tree crowns, (b) disk SE with a diameter of 7 pixels used for morphological opening operation on the crown, (c) the morphological opened image using disk SE in (b), (e) disk SE with a diameter of 9 pixels used for morphological opening of crowns in (d), (f) the morphologically opened image using disk SE in (e). A large disk SE removes the smaller crowns as well as the large upper branches of the larger crown.

In step 2, the treetops were identified and merged using the scales identified in step 1. As illustrated in Figure 5.2, at a given scale (at each iteration), the CHM was morphologically opened at the lower (i^{th}) and subsequent upper ($i^{th}+1$) scales. Local maxima were detected at both the scales to identify the cross-sections of tree crowns at the two scales. To determine which scale best represented a given tree crown, a Gaussian function shown in equation 5.2 was fitted for each identified treetop and the residuals were computed using equation 5.3.

$$G(x,y) = Ae^{-\left(\frac{(x-u_x)^2}{2\sigma_x^2}+\frac{(y-u_y)^2}{2\sigma_y^2}\right)} \quad (5.2)$$

$$SSE = \frac{1}{n-1}\sum_{i}^{n}[CHM_i - G(x_i,y_i)]^2 \quad (5.3)$$

Multi-scale analysis was then performed by analysing the residuals and selecting the optimal scale for the identified top. The decision to increment from lower (i^{th}) to upper ($i^{th}+1$) scales was based on comparison of the residuals at the two scales. If smaller residuals were observed at the upper scale, for an identified treetop, the scale was incremented, and a new treetop was initialized at the larger scale. If the residuals at the upper scale were however larger than the treetop at the smaller scale was retained.

There were two potential scenarios when merging treetops from two different scales: 1) the treetops identified at two adjacent scales were concentric (or approximately concentric), or 2) the treetops identified at the upper scale covered (or partially covered) multiple treetops at the lower scale. In the first scenario, the accuracy of treetop detection was invariant to the scale used to initialize the treetop, as at both upper and lower scales a tree crown was localized. However in the second scenario, the accuracy of treetop detection was entirely dependent on the scale. If at lower scales multiple treetops were correctly identified for a tree cluster, than at the upper scale those treetops were falsely merged together to represent a single crown. Conversely if at lower scales multiple treetops were falsely identified for a large tree crown than at the upper scales, those treetops were correctly merged together.

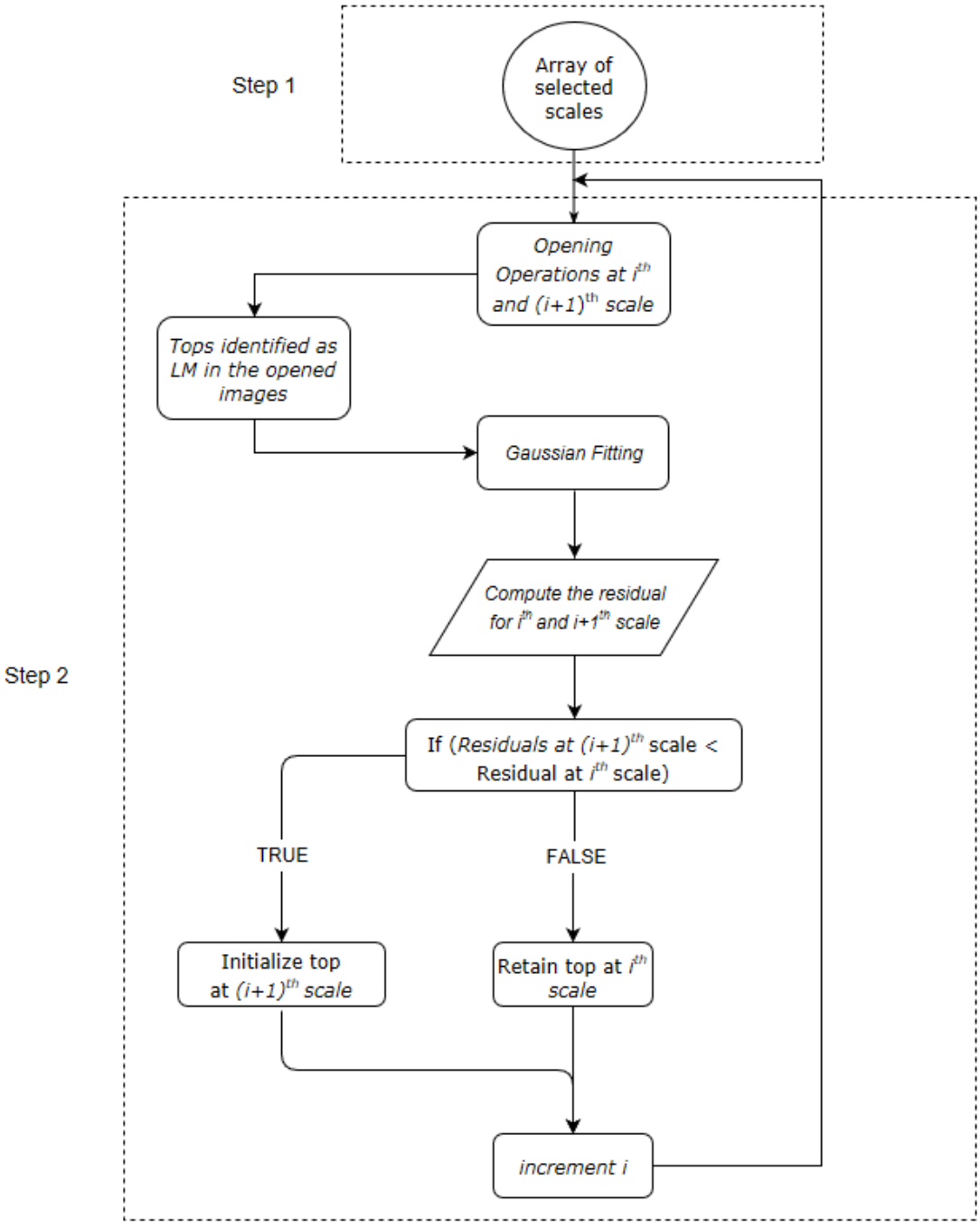

Figure 5.2. Improved multi-scale treetop detection flowchart. In step 1, the predominant crown sizes corresponding small, medium and large tree crowns are determined. In step 2, the tree tops are identified at each scale and merged using residual analysis.

5.3 Improved Region-based ITC Delineation

The identified treetops were used as seeds in a modified seeded region growing (SRG) algorithm to produce the final segments of the ITCs. The traditional SRG method was improved in the following aspects: (1) An improved contextual based homogeneity measure was proposed using the neutrosophic logic to mitigate the effect of spectral noise and integrate different intensity channels (Shan et al., 2008; Naveed and Hu, 2017). (2) A positional constraint based on the LiDAR information was employed to ensure that the growing region conformed to the Gaussian morphology of the tree crown, which effectively integrated the spectral and structural information of tree crowns in ITC delineation. In the following sections these two improvements are described in detail.

5.3.1 Homogeneity criterion based on Neutrosophic logic

Segmentation based on neutrosophic logic, was initially proposed by Shan *et. al.*, (2008), to extract lesions in ultrasound images. It was reported that by accounting for contextual information in ultrasound images, the effect of noise, commonly present in medical images, could be mitigated and the segment boundaries could be refined. Based on this notion, in this study, neutrosophic logic was used, for the first time, to mitigate the effect of noise in the intensity of the LiDAR data for ITC delineation. Neutrosophic logic introduces a degree of variance when evaluating the spectral similarity between two regions (Shan et al., 2008). The criteria for the addition of a pixel to a region depends on two quantities: degree of truth and level of indeterminacy. The degree of truth is the normalized spectral distance between the seeded region (i.e. segment) and the pixel under examination. The level of

indeterminacy introduces a measure of spectral variance of a small circular neighbourhood surrounding the pixel. A lower level of indeterminacy implies that the region surrounding the pixel is homogeneous, whereas a higher level of indeterminacy is indicative of a noisier region (Shan et al., 2008). In this study, to determine if a pixel could be merged to its neighbouring segments, a rule-based approach was used: if the degree of indeterminacy was smaller than a threshold value, the degree of truth of the individual pixel was calculated (Shan et al., 2008). A level of indeterminacy higher than the threshold value was indicative of a noisy region or presence of potentially another crown type in the surrounding and hence the degree of truth of a small circular region surrounding the pixel was calculated instead. A region with higher indeterminacy indicated a lower confidence in a single pixel alone to decide on the merge criteria and hence a small circular region was used as an approximation of the individual pixel instead. Equation 5.5, originally proposed by Shan et. al., (2008), describes the similarity metric used to merge pixels to the segments. Since the similarity metric was computed for three intensity channels, a combined metric was devised in equation 5.6 using the variance of the three channels. Equation 5.6 was proposed, in this study, to merge the individual similarity metrics for different intensity channels to compute a final variance weighted similarity metric. However, instead of using the variance over the entire spatial extent of the image, the variance for each band was computed around the locality of the growing region. The degree of truth of the individual pixels and their surrounding regions was then weighted and averaged based on the variances in each individual band ($\sigma_{C_i}^2$) in equation 5.6.

$$T'_{C_i}(x,y) = 1 - \frac{\left|\mu_{C_i} - \mu_R\right|}{\mu_R} \tag{5.5}$$

$$S(x,y) = \frac{\sum_i \frac{1}{\sigma_{C_i}^2} T_{C_i}}{\sum_i \frac{1}{\sigma_{C_i}^2}} \tag{5.6}$$

Wherein u_R and u_{C_i} represent the mean of the region surrounding the pixel (*x, y*) and the mean of the growing region in spectral channel *i*, respectively. $T'_{C_i}(x,y)$ is the degree of truth for a small circular region surrounding pixel (*x, y*). To compute the degree of truth for individual pixel ($T_{C_i}(x,y)$), the mean of the region surrounding pixel (*x, y*) (u_R) was simply replaced by the pixel value at location (*x, y*). The decision to compute the degree of truth for individual pixel or a small circular region was based on the degree of indeterminacy, shown in equation 5.7 below.

$$I_{C_i}(x,y) = 1 - e^{-\frac{\sigma_{C_i}^2}{100}} \tag{5.7}$$

The degree of indeterminacy was computed by using the variance of small region surrounding pixel (*x, y*) ($\sigma_{C_i}^2$) (Shan et al., 2008). If the degree of indeterminacy was below 0.5, the degree of truth of individual pixel was calculated. Otherwise the degree of truth of the small circular region around the pixel was used. For $T_{C_i}(x,y)$ a single threshold value of 0.6 was found optimal in successfully merging the pixels belonging to the growing regions. However, for $T'_{C_i}(x,y)$ a single threshold, as proposed by Shan et al., (2008), did

not work, as the degree of truth of a region was dependent on the variance of that region. Instead, in this study, a thresholding sigmoid function was constructed to make a more informed merge decision. The input to the sigmoid function was $I_{C_i}(x,y)$ and the output was a threshold value for the $T'_{C_i}(x,y)$. The sigmoid function is shown in equation 5.8.

$$F_{sigmoid} = \left(\frac{A * I_{C_i}(x,y)}{1 + e^{-B\left(I_{C_i}(x,y)+C\right)}} \right)^{1-I_{C_i}(x,y)} \tag{5.8}$$

The values of A and B controlled the scale and the steepness of the sigmoid curve. The value of C was used to adjust the inflection point at which the curvature of the curve changes. In this study the values of A and B were set to 1 and the value of C was 4.5. If $T'_{C_i}(x,y)$ exceeded the threshold value determined from the sigmoid curve the pixel was merged to its respective segment.

5.3.2 LiDAR Shape Constraint

The positional information in the LiDAR was used to morphologically refine the boundaries of the crown and prevent over-segmentation in dense tree clusters. The tree crowns in the CHM could be modelled by a Gaussian function. As a result the morphology of the crown, exhibited in the CHM, was exploited during the region growing process to constrain the growing regions to follow a Gaussian shape.

In the implementation of the SRG algorithm, the 8-connected neighbouring pixels of a region were checked for spectral similarity using neutrosophic logic; however an additional constraint on the elevation was also enforced to ensure morphological similarity. Using the CHM the immediate 8-connected neighbouring pixels of a growing region were compared with the outermost contour of the region. Figure 5.3 illustrates the schematics of the method.

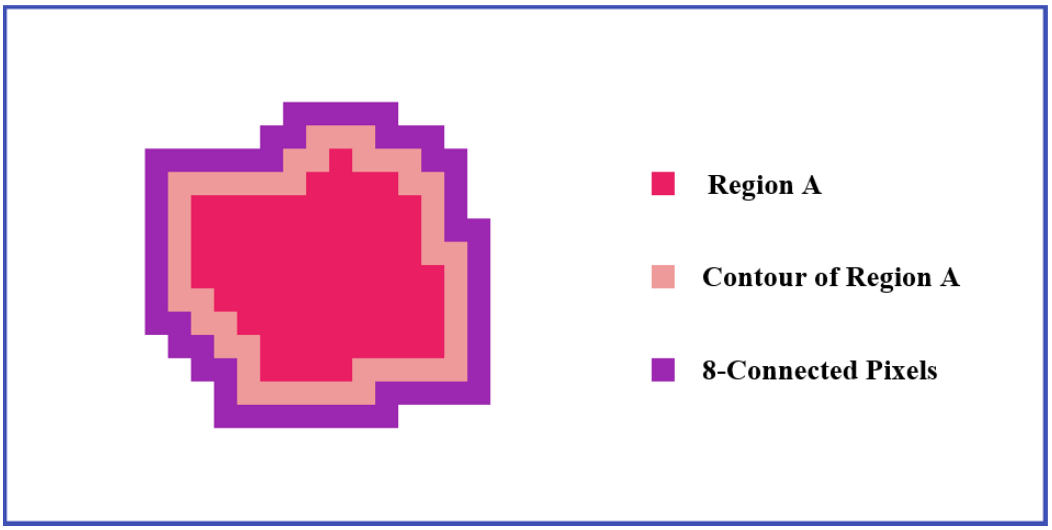

Figure 5.3. The difference in elevation illustrated between the outer most contour of a region with the 8-connected neighbouring pixels.

The difference in the elevation was then checked against a threshold buffer zone. The immediate neighbours were considered as valid if the absolute difference between the pixel and the outer most contour was within a given threshold. This behaviour was modelled upon the idea that from the initially identified treetop, the neighbouring points would reflect a general decreasing trend in elevation until the boundary of the crown (Figure 5.4). In the case of tree clusters, any sudden change in the elevation would indicate the presence

of another crown and hence the pixel would not be considered as a valid neighbour for the growing region.

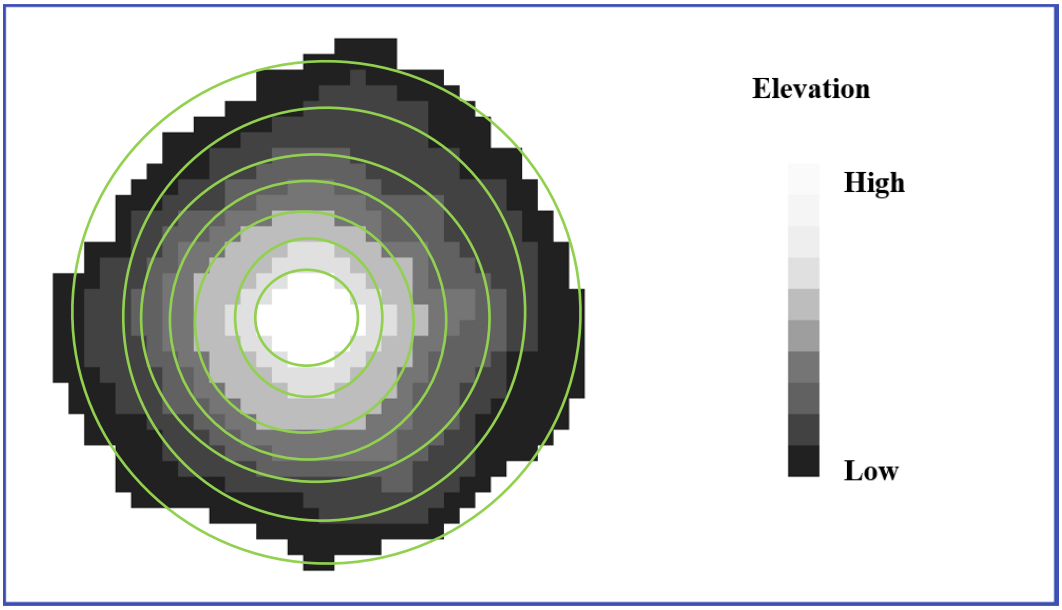

Figure 5.4. Nadir view of the tree crown in the CHM filtered to represent first returns. The elevation gradually decreases from the top of the crown (i.e. the treetop) to the boundary of the crown. The contour lines illustrate points (pixels) of constant elevation in the CHM. The inner most contour represents the highest elevation just around the treetop and the outermost contour represents the lowest elevation around the boundary of the crown.

This morphological constraint was found to be most applicable to CHM based ITC delineation approaches as the subsequent returns, which could represent inconsistent elevation trends within a single crown, were removed. Furthermore, the effect of scan lines and noise in the CHM was also removed by prior smoothing applications.

5.4 ITC Delineation Accuracy Assessment

The segmentation accuracy assessment was performed by comparing the results of the proposed region-based segmentation algorithm with the manually delineated reference polygons illustrated in section 3.3. The final accuracy metrics were computed by examining the overlap ratio between the delineated results and the corresponding reference polygons in the ground truth dataset using equation 5.9.

$$Overlap = \frac{Area(Segment \cap Reference\ Polygon)}{Area(Segment)} \tag{5.9}$$

The overlap ratio between the delineated results and the reference polygon was computed and compared against threshold values. An overlap ratio of greater than 50% was considered a 1:1 match. An overlap ratio of less than 50% but greater than 25% was considered a partial match; and an overlap ratio of less than 25% was considered near complete omission. Based on these accuracy metrics, the following three different variants of the proposed method were examined.

Method 1: Treetop detection with improved multi-scale method and crown boundary delineation with intensity data and CHM. It is referred as the original method hereafter.

Method 2: Treetop detection with improved multi-scale method and crown boundary delineation with intensity data. Method 2, hereafter, is referred as the Neutrosophic method using intensity data only.

Method 3: Treetop detection with improved multi-scale method and crown boundary delineation with CHM. Method 3 is referred as the Neutrosophic method using CHM only.

The first method was the method proposed in this study to uniquely exploit the intensity and positional data from the Titan LiDAR. The second evaluation (i.e. method) was used to check the effectiveness of combining positional information from the LiDAR with the LiDAR intensity data. With LiDAR shape constraint, the growth of individual regions was constrained by an elevation threshold in the CHM and hence the boundaries of the segments were refined to the morphology of the crown. Hence with the second method, the effectiveness of the positional constraint on the quality of the segmentation was examined by only segmenting the ITCs using the intensity information with neutrosophic logic (i.e. the LiDAR shape information was not used). The third method was added to check the applicability of neutrosophic logic using the LiDAR shape information itself. Hence in the third method, the intensity data was completely ignored and the positional information in the CHM was exploited to perform the segmentation using neutrosophic logic. The results derived from the proposed method and its variants were also compared with the Meyer's flood fill variant of MCW segmentation. MCW segmentation is commonly exploited in ITC delineation and has been popularly reported to produce high accuracy metrics particularly with LiDAR data (Chen et. al., 2004; Jing et. al., 2012). The MCW method was tested with LiDAR and intensity information, individually and combined. The three variants of MCW segmentation used in this study are as follows:

1) MCW segmentation with intensity data and CHM

2) MCW segmentation with intensity data

3) MCW segmentation with CHM

Additionally, the proposed region growing segmentation method was also judged independently of the improved multi-scale treetop detection method. Since the accuracy of the ITC delineation framework was exclusively dependent on the initial treetop detections, it was difficult to independently judge the segmentation results. To circumvent the loss of accuracy due to false treetop detection, reference treetops were generated using the manually delineated polygons. ITCs were then segmented using the reference treetops and the results were compared with the manually delineated crowns. Since reference treetops were used, the treetop detection accuracy was 100% and the overlap ratio metrics were exclusively reflective of the quality of segmentation. To generate the reference treetops, the manually delineated segments were individually isolated by converting the vectors (i.e. shapefiles) into individual rasters. Each raster, representing a single ITC, was then further processed to extract the contours which were subsequently used to compute the centroid coordinates of the reference polygon. The centroid coordinates were then used to initialize a disk with a radius of 5 pixels to create reference tree tops. The following variants of the method were examined with reference treetops.

1) Reference treetops with crown boundary delineation with intensity data and CHM

2) Reference treetops with crown boundary delineation with intensity data

3) Reference treetops with crown boundary delineation with CHM

CHAPTER 6

RESULTS AND DISCUSSION

6.1 Multi-scale Treetop Identification

In this study, scale analysis, described in Chapter 5, was applied to the Titan CHM to identify the predominant crown sizes (i.e. scales) in the scene. The plot of the averaged differenced opened CHMs versus the diameters of the SEs used for opening operation is shown in Figure 6.1. A local minima was observed whenever there were significant differences in crown sizes between two successive opened CHMs (Jing et al., 2012). As shown in Figure 6.1, several minima were observed; the ones corresponding to the predominant crown sizes are marked with red circles. The first minima, corresponding to the diameter of the SE of 3 pixels was interpreted to be the result of upper tree branches and thus was excluded from the analysis.

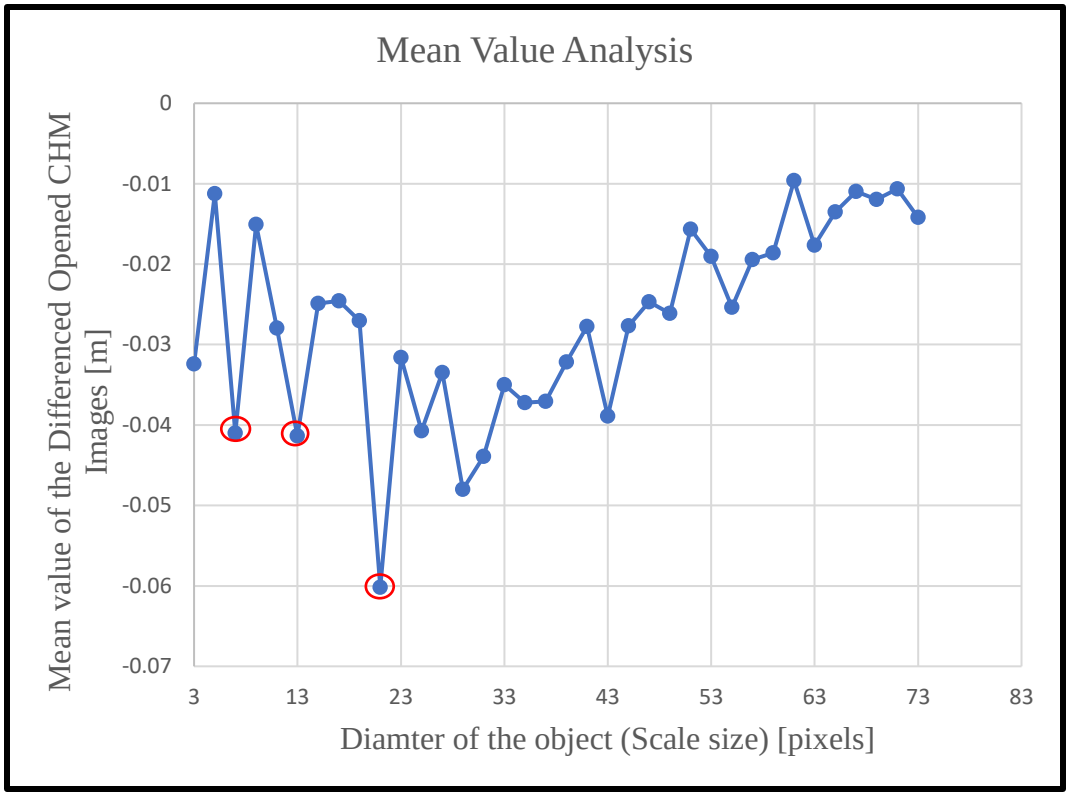

Figure. 6.1 Mean value analysis of the differenced opened CHM images at multiple scales. The scale (i.e. the diameter of the disk structuring element) was incremented with a gap of 2 pixels with a starting scale of 3 pixels and final scale of 73 pixels. The local minima, corresponding to the predominant crown sizes, are indicated by red circles. The final scales identified from the mean value analysis were 7, 13 and 21.

The local minima beyond the diameter of 21 pixels were subdued and were hence interpreted to represent tree clusters in the scene. Scale sizes of 7, 13 and 21 pixels were identified as representing the predominant crown sizes corresponding to small, medium and large tree crowns in the scene. The identified scales were used to generate the morphologically opened CHM images and consequently the local maxima were detected as the treetops in the opened images. Figure 6.2 shows the treetops identified at the scales of 7, 13 and 21 pixels. A small subset of the area is shown to better visualize the treetops at different scales.

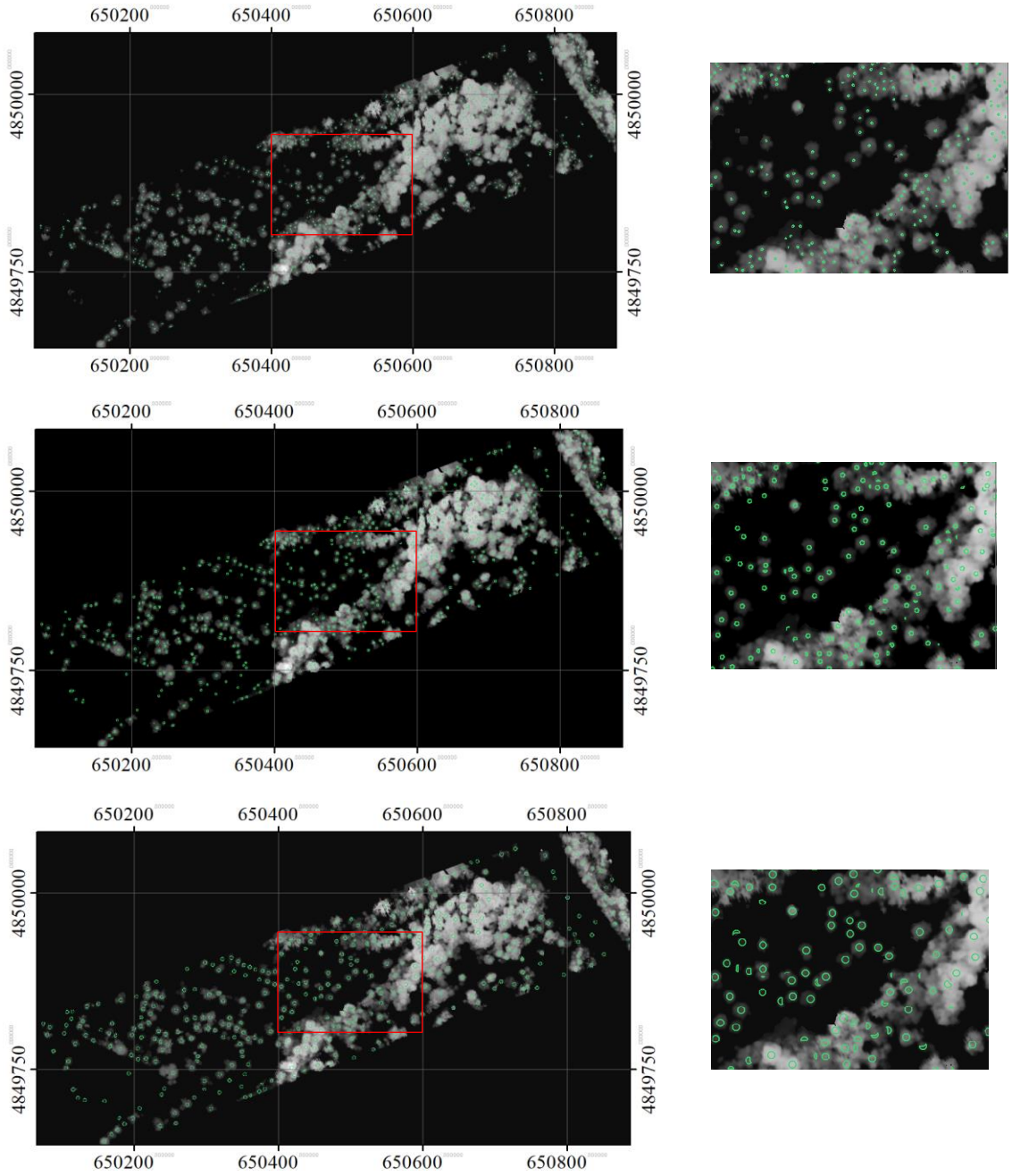

Figure. 6.2 The identified local maxima in the opened images. The results have been overlaid on the masked CHM. (*Top*: LM identified in the morphological opened image with a disk SE with diameter of 7 pixels, *Middle*: LM identified in the morphological opened image with a disk SE with diameter of 13 pixels, *Bottom*: LM identified in the morphological opened image with a disk SE with diameter of 21 pixels).

The individually identified local maxima were integrated using the improved multi-scale method. The resulting treetops after merging the individual treetops from different scales are shown in Figure 6.3.

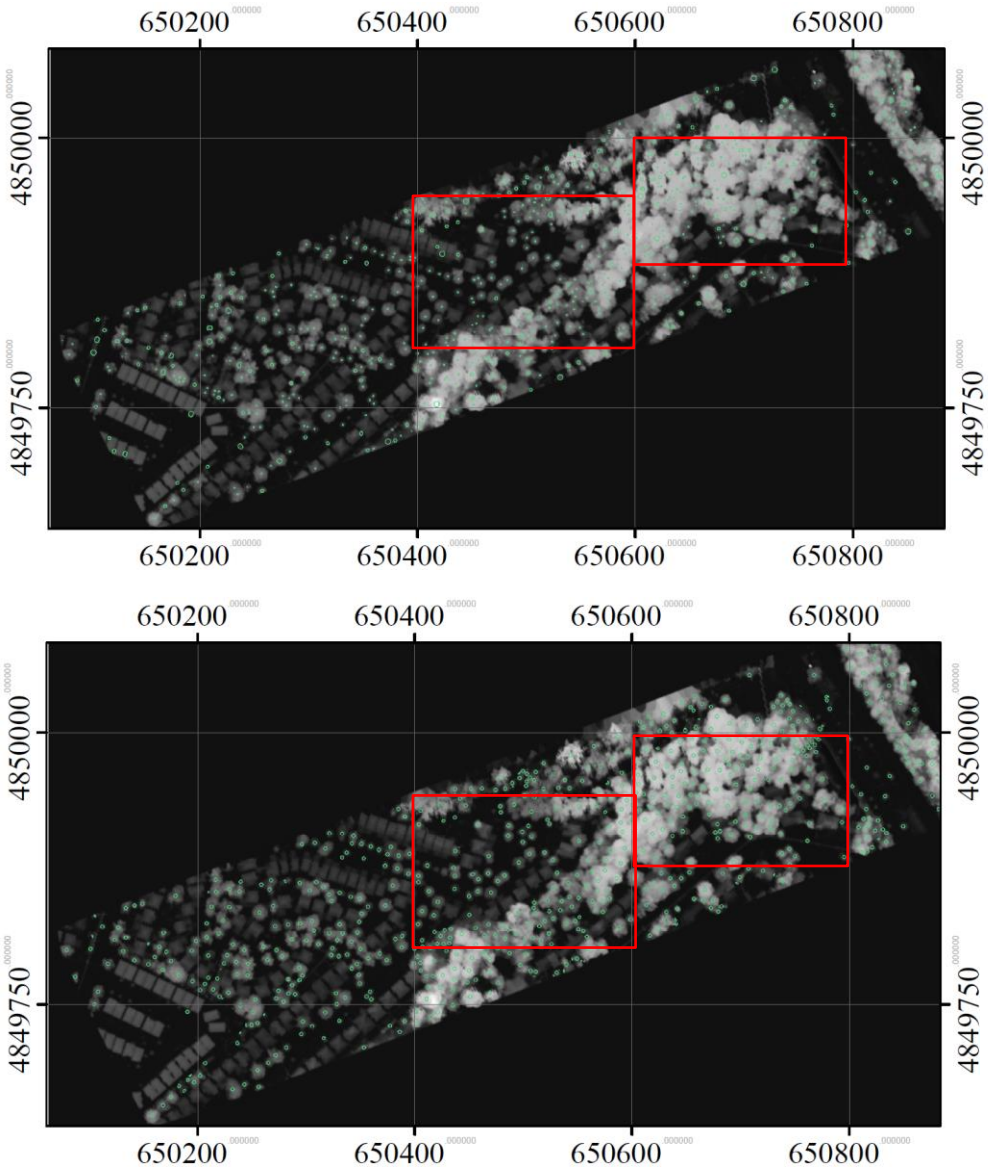

Figure. 6.3 The treetops identified as local maxima in the morphologically opened images. The tops were detected at scale of 7, 13 and 21 pixels. (Top: treetops detected using multi-scale method, bottom: reference treetops). The zoomed in regions are shown in figure 6.4.

Visual observation of Figure 6.3 indicated that most tree tops were identified correctly. This was especially true for trees in the residential areas, but in the woodlot area (marked by red squares in Figure 6.3), a higher commission error was observed. To illustrate this, the zoomed image of the areas marked by red squares in Figure 6.3 is shown in Figure 6.4.

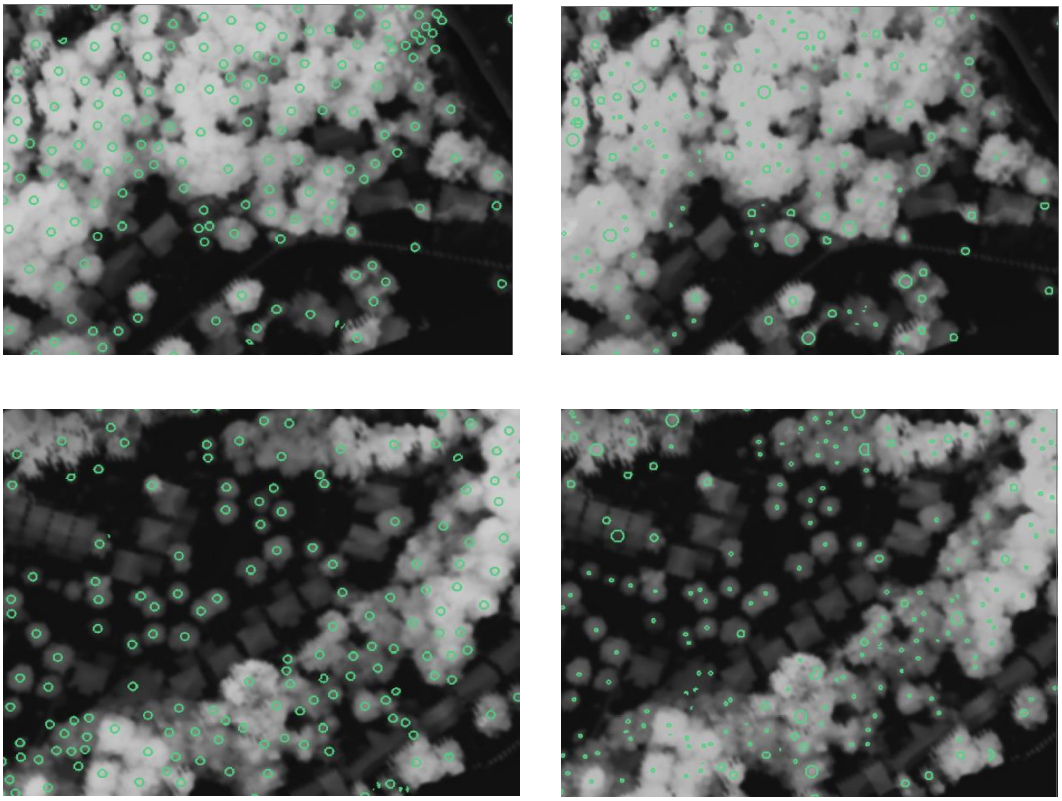

Figure. 6.4 Zoomed in map of the multi-scale treetop identifications evaluated against the reference treetops. The top row shows the treetop identification results in a dense stand and the bottom row shows the treetop results in an urban area. The reference treetops are shown in the left image and multi-scale results are compared in the right image.

The treetop detection results were analysed with respect to the two potential scenarios described in Chapter 5. In the case, where a single treetop was initialized at both upper $(i + 1)$ and lower (i) scales, the decision to increment the scale was based upon the fit of the

Gaussian template to the CHM, at each scale. If the template at upper scale yielded smaller residuals than a treetop at the upper scale was initialized. Otherwise the treetop at the original smaller scale was retained. This did not directly affect the accuracy of treetop detection, as at both upper and lower scales the tree crown was correctly localized.

In the case where the detected treetops at upper scale $(i + 1)$ covered or partially covered multiple treetops identified at the lower scale (i), the sum of the squared residuals was computed for the treetops at lower scale and compared with the residual of the treetop detected at upper scale. If the residual at upper scale was smaller than the sum of the residuals, for treetop at lower scale, than a single treetop was initialized at the upper scale. This scenario was commonly observed for large deciduous crowns, where at smaller scales, multiple treetops were falsely detected and at the upper scale a single treetop was correctly identified. However, for large crowns, multiple treetops were initialized at smaller scales (for the single tree crown) which may not have been merged at larger scales. This was due to the spatial distribution of the identified treetops: for large deciduous tree crowns with complex upper branch structure multiple treetops were identified away from the centre of the crown (i.e. closer to the crown edges). At larger scales, these treetops could not be merged due to their spatial distribution and hence this yielded a higher commission error in some areas. A few cases of such spatial distribution are shown in Figure 6.5.

Furthermore, the multi-scale method relied on the assumption that the treetops could be modelled by a Gaussian function. The validity of the Gaussian assumption was not completely accurate in accounting for irregular shaped large deciduous crowns in dense

clusters. At larger scales, the treetops would generally yield higher residuals due to structural irregularities in the shape of large deciduous crowns. This effect contributed to a higher commission error as the false treetops at smaller scale could not be merged together at upper scales.

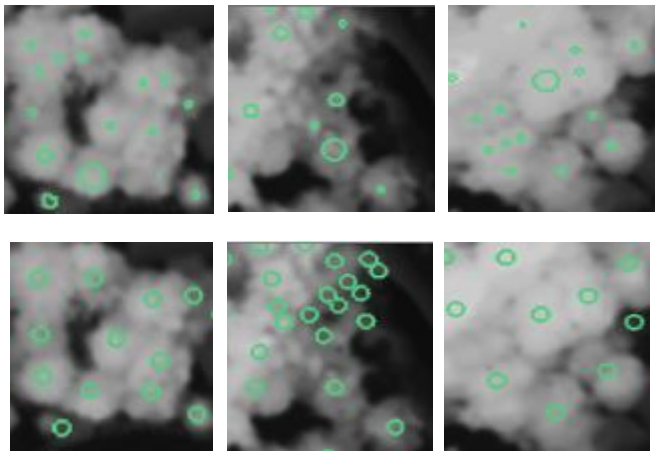

(a) (b) (c)

Figure 6.5. Identified treetops using the improve multi-scale method (top row) and the reference treetops generated as the centroid of the manually delineated polygons (bottom row). (a, c) The upper branches of the tree crown were falsely detected as treetops at the lower scale. Since the distribution of the false tops was away from the centre of the crown (where the true treetop was located), they could not be merged into a single top at the upper scales. (b) In some cases the treetops were falsely omitted when the crown was thinned and a local maxima could not be located at the given scale.

6.2 ITC Delineation with Multi-scale Treetop Identification

The identified treetops, presented in Section 6.1, were used to perform the ITC delineation using the improved seeded region growing algorithm. The results of the original method (using both intensity data and CHM) and its two variants (using CHM only and using intensity data only) are shown in Figures 6.6, 6.7 and 6.8, respectively. For comparison, a zoomed in portion of the original area (outlined as the red bounding box) is illustrated in Figure 6.9.

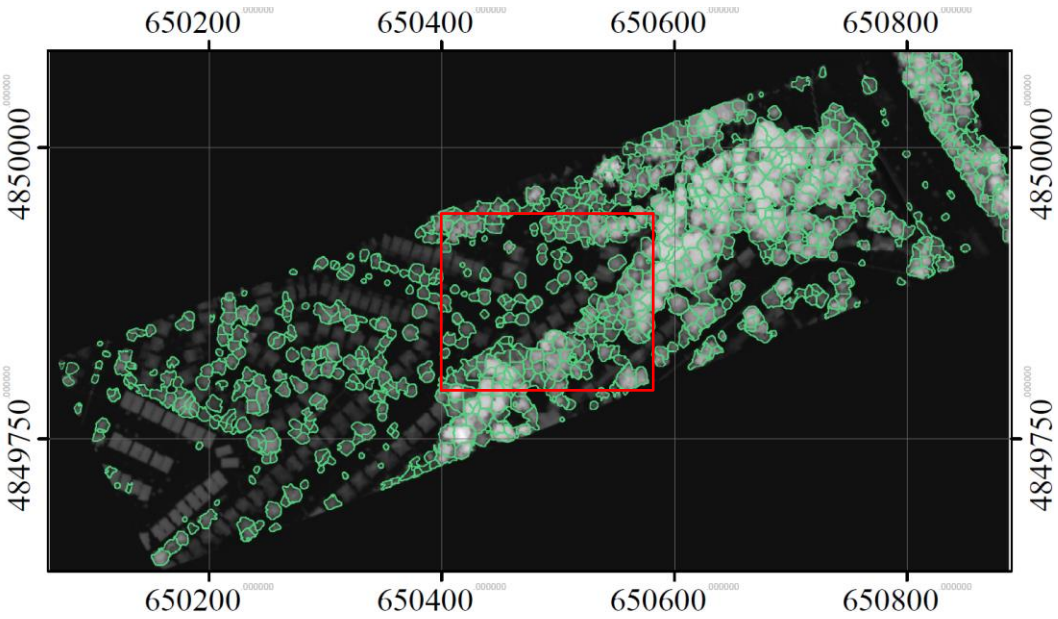

Figure 6.6. The delineated segments using the original method with CHM and intensity data. The intensity data was used to perform the segmentation using neutrosophic logic and the CHM was used to enforce the LiDAR shape constraint. A zoomed in portion of the area (in the red bounding box) is shown in Figure 6.9.

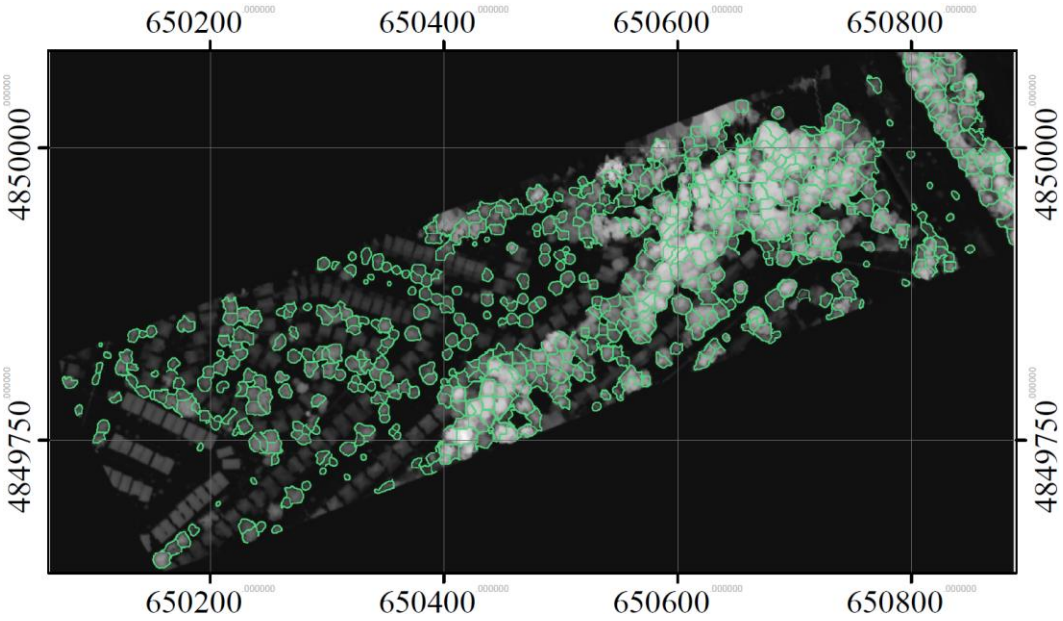

Figure 6.7. The delineated segments generated using the neutrosophic method with CHM only.

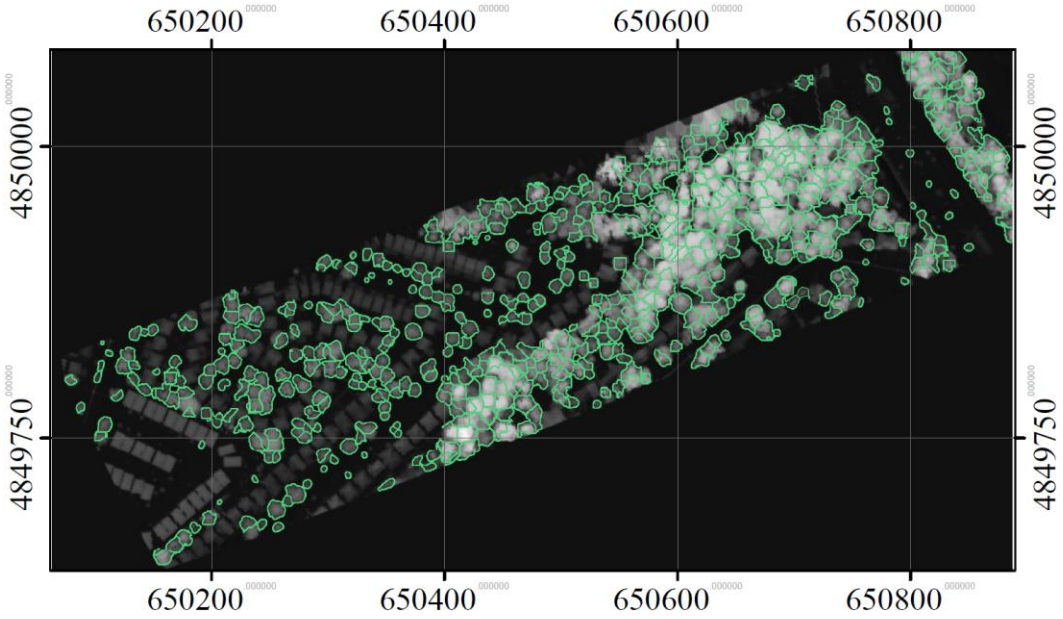

Figure 6.8. The delineated segments generated using the neutrosophic method with intensity data.

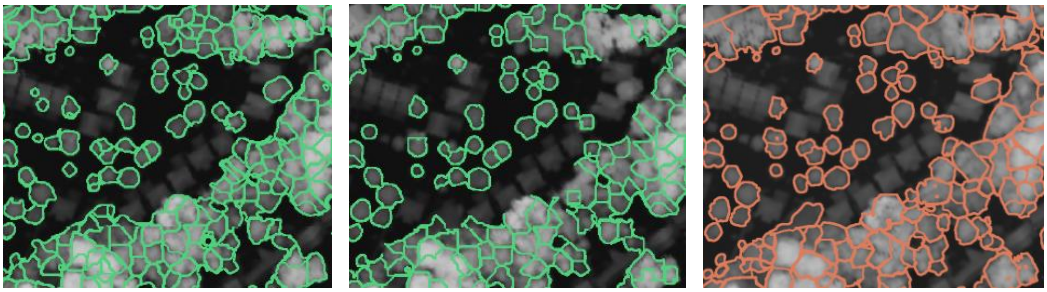

Figure 6.9. Zoomed in region of the delineated segments. (Left: original method (using CHM and intensity data), middle: neutrosophic method (using CHM), right: reference polygons.

From these figures, it can be observed that the results generated by the original method (using intensity data and CHM) were a better match to the reference delineation results as compared to its other two variants. Furthermore, the crown boundaries generated via the original method were more refined and closely approximated the reference boundaries of the tree crown relative to those generated by the other two variants. Even though, for the neutrosophic method using CHM only, the boundaries of the delineated ITCs were also observed to follow the morphological boundaries of the crown, cases of under segmentation were commonly present. In comparison, the variant using only the intensity data had the worst performance out of the three methods with the delineated ITCs not conforming to the structural boundaries of the crown. These observations were consistent with the quantitative results shown in Table 6.1.

Table. 6.1 Accuracy metrics for ITC delineation using the proposed seeded region growing method and its neutrosophic variants. The initial approximations of the treetops were derived from the improved multi-scale method with scales 7, 13 and 21 corresponding to small, medium and large tree crowns. There were a total of 718 manually delineated tree crowns in the study area. The results were compared with similar variants of MCW segmentation.

ITC Delineation Method	1:1 Match	Partial Match	Omitted
Original method using Intensity and CHM	414	107	197
Neutrosophic method using CHM	407	109	202
Neutrosophic method using Intensity	404	89	225
MCW using CHM	323	177	218
MCW using Intensity	269	143	306
MCW using CHM and Intensity	327	164	227

The obtained results on average reflected a combined ~70% 1:1 and partial match to the reference polygons for the original method and its two neutrosophic variants. For the original method (using CHM and intensity data), 57.7% of the crowns were a 1:1 match and 14.9% of the delineated ITCs were a partial match. For the method without spectral information (i.e. Neutrosophic method (using CHM only)) and the method without LiDAR positional information (i.e. Neutrosophic method (using intensity data only)) 56.7% and 56.2% of the delineated ITCs were a 1:1 match and 15.2% and 12.4% of the ITCs were a partial match, respectively. It was observed that several segments were also completely omitted in the delineated results (~29% on average from all 3 methods). The results indicated that the original method (using CHM and intensity data) had the highest number of 1:1 matched crowns. The original method (using intensity data only) ranked the lowest among the three original methods with the highest number of complete omissions.

A 12% increase, in 1:1 matched crowns, was observed with the original method over the MCW segmentation (using intensity data and CHM). Other variants of the MCW segmentation had lower accuracies with MCW (using intensity data) having the lowest 1:1 matched crowns and the highest number of complete omissions. Though the original method generally outperformed the MCW method, the results of the three proposed seeded region growing variants indicated that the intensity information alone was not sufficient in obtaining accurate ITC delineation results. In both variants of the original and MCW segmentation methods (i.e. neutrosophic method (using intensity data) and MCW (using intensity data)) the intensity information produced the lowest accuracy metrics with the highest number of complete omissions. In comparison the variants using the CHM yielded higher accuracies with fewer complete omissions. For the neutrosophic method, however, the difference between the intensity (a total of 404 1:1 matched crowns) and CHM (a total of 407 1:1 matched crowns) variants was not significant. This was attributed to the incorporation of the contextual information in the neutrosophic logic based merge criterion during region growing. Since a contextual based similarity metric was used, the presence of noise in the intensity data was mitigated to generate more accurate segmentation. In comparison, no such criterion was present in the flood fill variant of the MCW segmentation and hence the derived results were poor.

For all variants of the original and MCW methods, a high number of completely omitted crowns were observed. This was primarily attributed to the erroneous treetop detections. There were two popular scenarios that led to low accuracies for 1:1 matched ITC segment and consequently a higher number of complete omissions. The first scenario, though not

as prevalent in this study, was the complete omission of the treetops in the treetop identification phase. If a treetop was falsely omitted (i.e. the crown was not localized) then the crown was never segmented. Majority of the studies reported the initial treetop omission as a major source of error for under-segmentation in dense forest stands and isolated tree crowns in urban environments alike. Although this was not as commonly observed in this study, due to the incorporation of the multi-scale method, there were still instances where the initial treetop omission in dense tree clusters and for isolated individual crowns contributed to the under-segmentation or complete omission of certain ITCs.

The second and a more relevant factor for low accuracy metrics was the large commission error in the treetop detection module. The false identification of multiple treetops for a single crown led to multiple segments intersecting a common reference polygon. There were two possible scenarios that arose when multiple segments intersected a common reference polygon: 1) at least 1 segment had an overlap ratio of greater than 50%, which indicated that the segment could be considered as a 1:1 match for the reference polygon, 2) none of the segments could be considered a 1:1 match (i.e. all the segments were a partial match). Figure 6.10 illustrates the instances where the two cases are encountered.

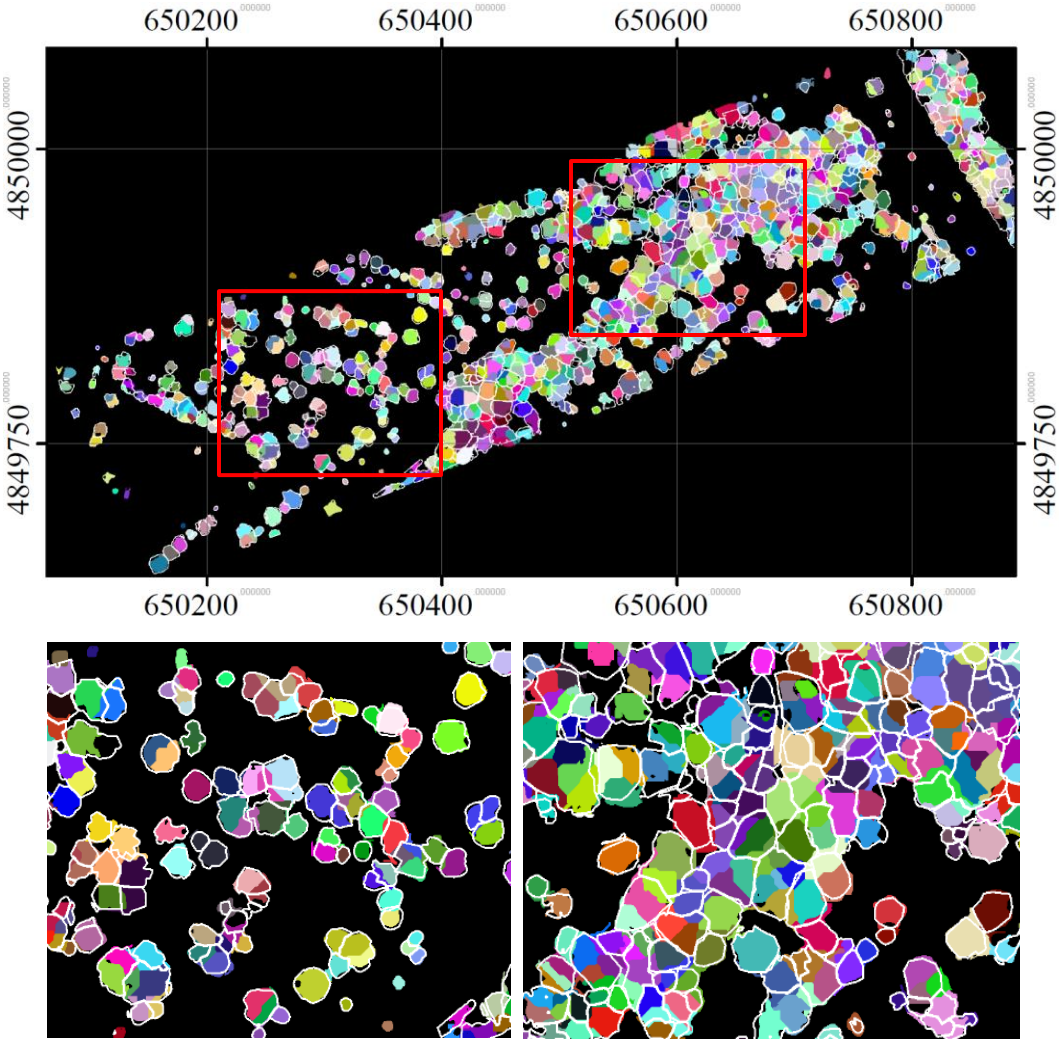

Figure 6.10. The delineated segments generated using the original method (using CHM and intensity data) with reference polygons with white boundaries overlaid on top. A zoomed in area (marked by red boxes) is shown to illustrate the cases of multiple segments intersecting a reference polygon.

Since the erroneous treetop detections were more prevalent in the dense forest stand, a higher number of multiple segments intersecting a common reference polygon were observed in this region. In the case of multiple false detections, it was also observed that the LiDAR shape constraint did not prevent the erroneous growth of the regions as each identified top represented a local maxima at the selected scale. Hence the immediate region

around the top conformed to the Gaussian function which prevented the effective use of LiDAR positional information in stopping the erroneous growth of the region. This effect is demonstrated in Figure 6.11 below.

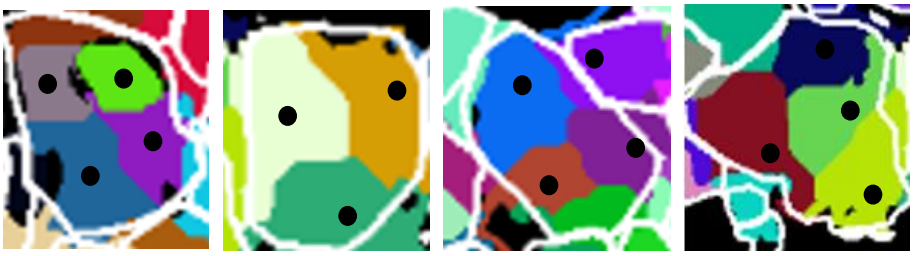

Figure 6.11. Cases of multiple segments intersecting a common reference polygon (shown as the white boundary). The initial identified treetops from the proposed multi-scale method are shown with black circles. If any one of the multiple segments had an overlap ratio of greater than 50% with the reference polygon, it was considered as a 1:1 match and the other segments were discarded. In the case where none of the segments could be considered as a 1:1 match, the segment with the highest overlap was considered as a partial match and the rest were discarded. If none of the segments could be considered as 1:1 or partial matches, then the segment was considered as a complete omission.

Though multiple false treetop detections contributed to a lower segmentation quality, it was observed that even in the case of multiple segments being identified for a single crown, the boundaries of those multiple segments still conformed to the structural boundaries of the ITC. In Figure 6.11, though multiple segments represented a single crown, the joint boundary of the multiple segments generally conformed to the structural boundary of the ITC. This was however not the case for multiple segments being identified due to over-segmentation from neighbouring regions. The over-segmented crowns had a high overlapping ratio; however this came at the cost of neighbouring segments being under-segmented due to the over growth of certain regions in areas of dense tree clusters. Hence

it was observed that the two quantities were correlated with one another particularly in dense tree clusters.

6.3 ITC Delineation with Reference Treetops

To assess the accuracy of the ITC delineation framework independently of the multi-scale treetop detection method, reference treetops were used as initial seeds for the proposed region-based segmentation method. Hence the accuracy for the treetop detection was assumed to be 100%. The results for the ITC delineation framework with reference treetops are shown in Figures 6.12, 6.13 and 6.14. The overlap ratio metrics are shown in Table 6.2.

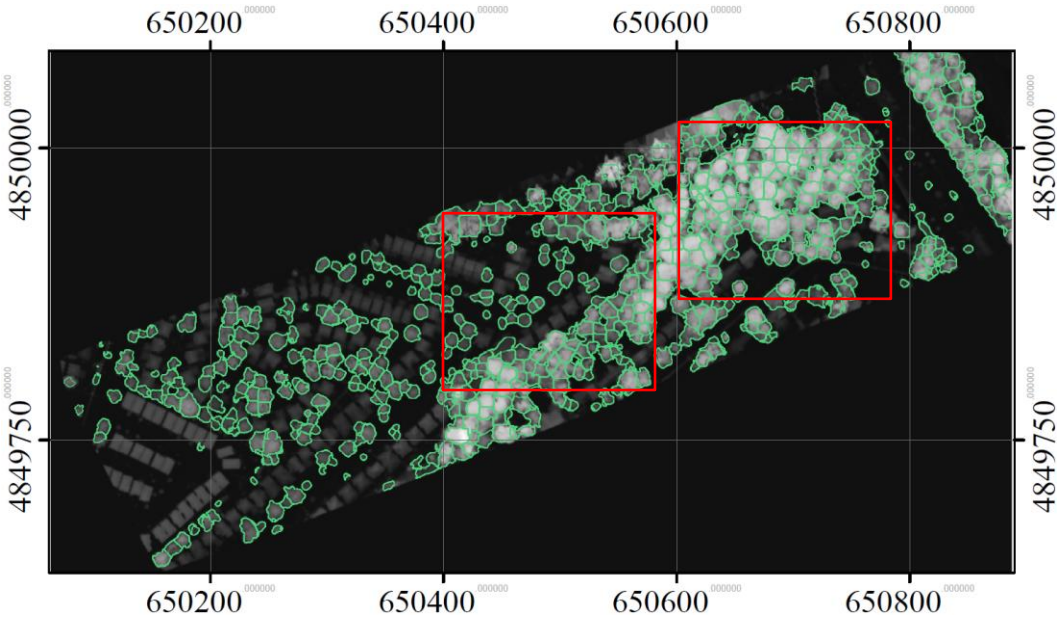

Figure. 6.12 The delineated segments using the original method with CHM and intensity data. Reference treetops with a radius of 5 pixels were used as the initial seeds for the region growing. A zoomed in portion of the area (in the red bounding box) is shown in figure 6.15 with reference polygons overlaid.

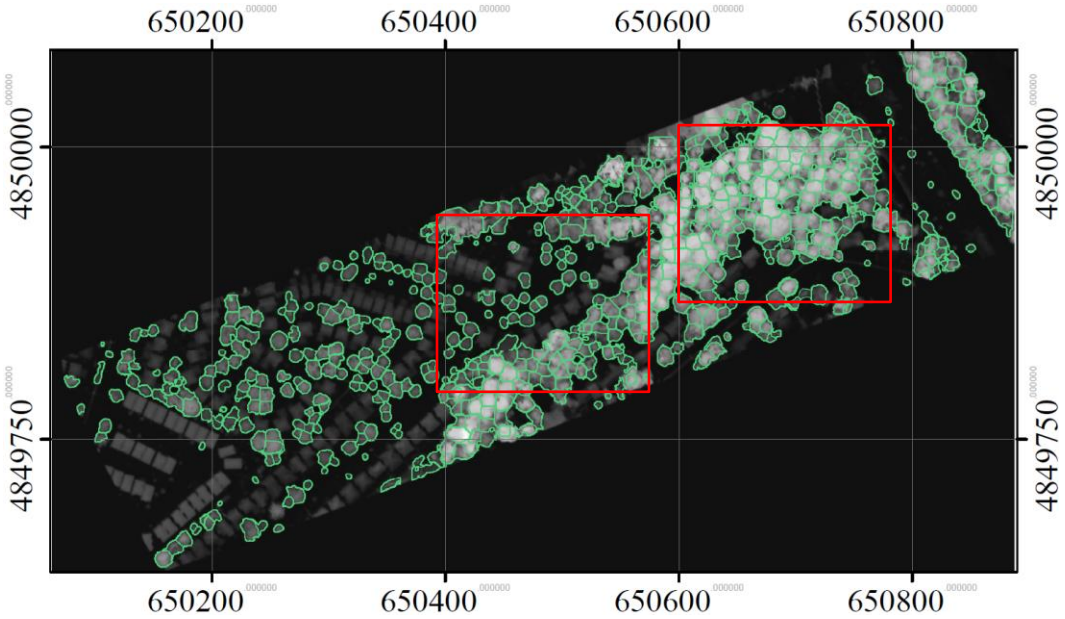

Figure. 6.13 The delineated segments generated using the neutrosophic method with CHM only. Reference treetops were used as the initial seeds.

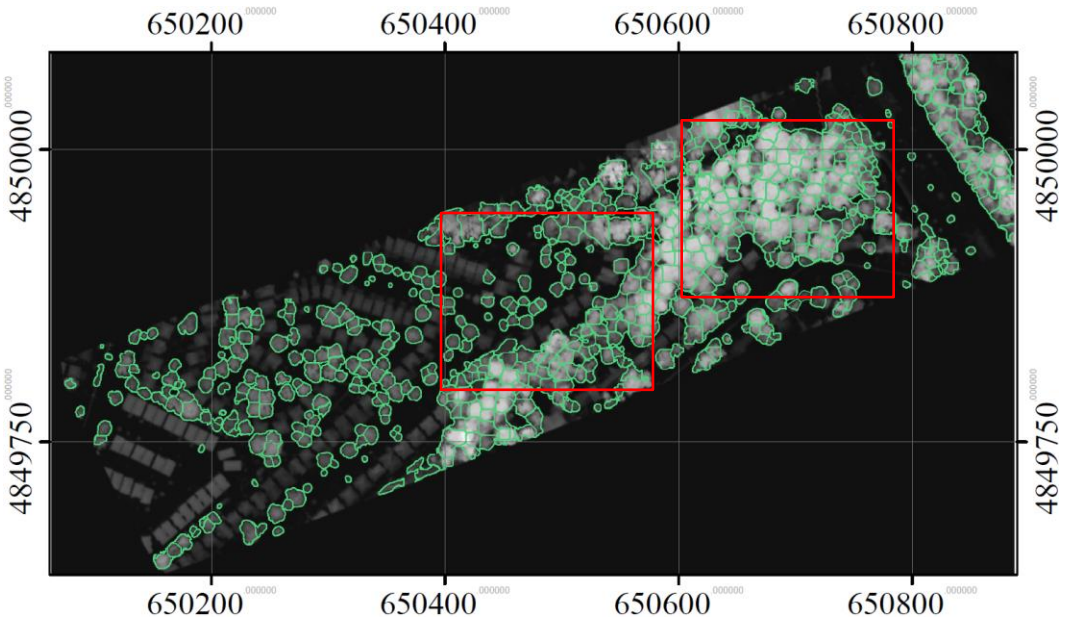

Figure. 6.14 The delineated segments generated using the neutrosophic method with intensity data only. Reference treetops were used as the initial seeds.

The results indicated that a significantly higher number of delineated segments were a 1:1 match as compared to the ITC delineation with multi-scale treetops. Furthermore the boundaries of the delineated segments were also aligned with the structural boundaries of the crown in the CHM. The accuracy metrics for overlap ratio are quoted in Table 6.2 below.

Table. 6.2 Accuracy metrics for the ITC delineation with reference treetops. Results from the original method, its neutrosophic variants and MCW segmentation are illustrated. The centroids of the reference polygons were used as reference tree tops with a radius of 5 pixels. A total of 718 reference treetops were generated from the reference polygon.

ITC Delineation Method with Reference Tree Tops	1:1 Match	Partial Match	Omitted
Original method using Intensity and CHM	635	16	67
Neutrosophic method using CHM	628	14	76
Neutrosophic method using Intensity	608	17	93
MCW using CHM	596	66	68
MCW using Intensity	604	58	68
MCW using CHM and Intensity	605	58	67

For the original method (using CHM and intensity data) a total of 88.4% of the crown were a 1:1 match with the reference polygon and 9.33% of the crowns were completely omitted. In comparison 87.4% and 84.7% of the total 718 crowns were a 1:1 match and 10.6% and 13.0% of the crowns were completely omitted for neutrosophic method (using CHM) and the neutrosophic method (using intensity data), respectively. The results were significantly improved with the reference treetops and fewer cases of over and under segmented crowns were present. Figure 6.14 illustrates the zoomed-in-area of the segmented regions from the three variants of the original method with reference polygon overlaid.

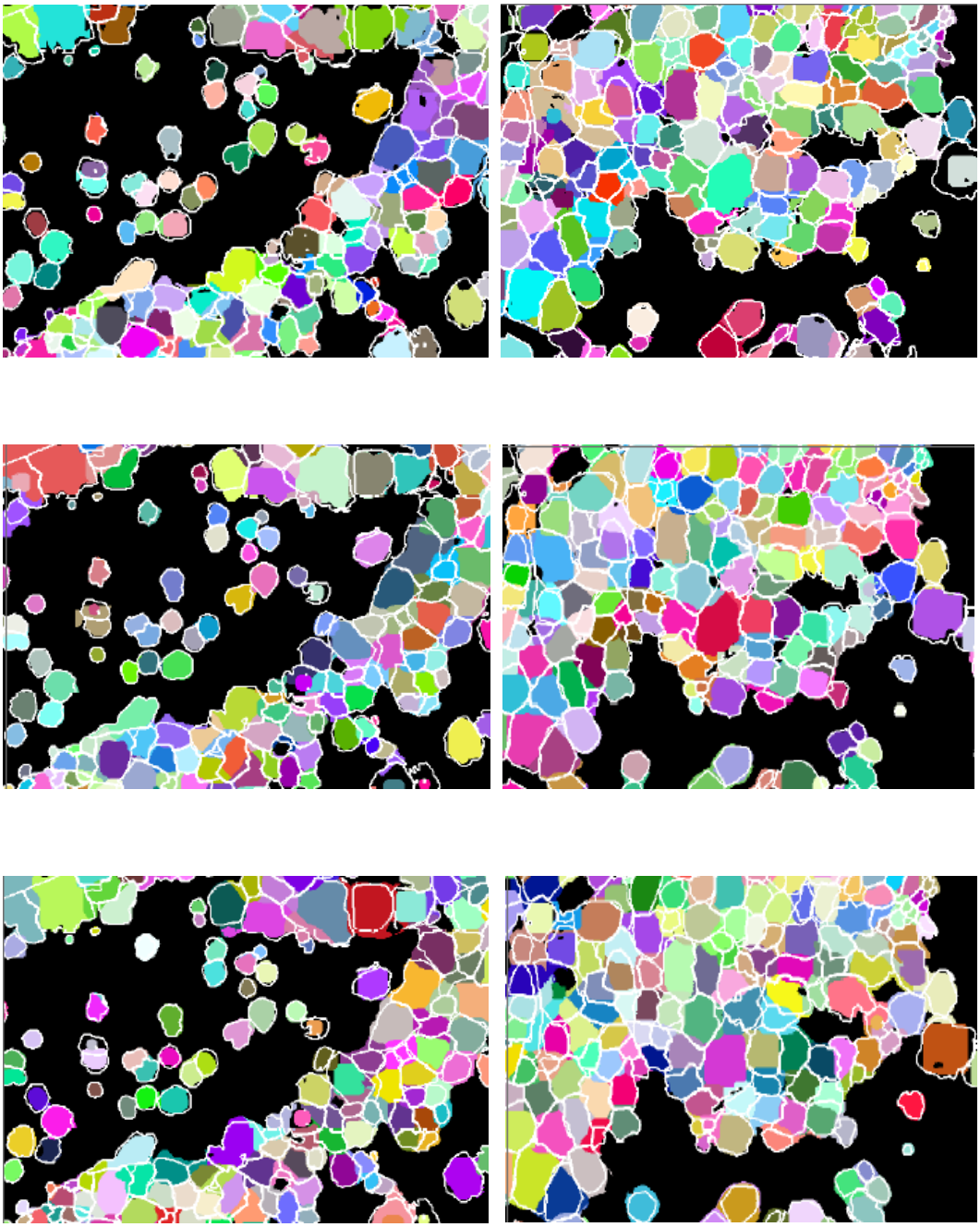

Figure 6.15 The zoomed-in regions from figures 6.12, 6.13 and 6.14. The reference polygons with white boundaries have been overlaid on the coloured region growing segments (top row: original method (using CHM and intensity data), middle row: neutrosophic method (using CHM), bottom row: neutrosophic method (using intensity data).

From the results in Figure 6.15, all three variants of the original method produced regions that generally conformed to the structural boundaries of the crown. However for the neutrosophic method (using intensity data only), the boundaries of the segmented regions generally conformed to the spectral boundaries of the crown as there was no structural parameter used in the region growing process. For this reason the observed accuracy metrics were also lower than the other variants. In comparison with MCW segmentation (using CHM and intensity data), the original method (using CHM and intensity data) had a 4.2% improvement in 1:1 matched crowns. The number of complete omissions were however the same. The other variants of MCW had similar results with MCW (using CHM) having the lowest 1:1 matched crowns. In terms of the quality of segmentation, the original method (using CHM and intensity data) had lowest cases of over and under segmentation. The general trend of the observed results indicated that neutrosophic logic was able to yield better segmentation results by incorporating a measure of contextual information in the merging criterion during region growing. The neutrosophic logic based merging criterion was also demonstrated to work on CHM, however, the incorporation of LiDAR shape constraint was demonstrated to be a better metric for exploiting the positional information in the CHM.

The accuracy metrics used in the study gave a macro assessment of the quality of segmentation. Additional metrics to provide a pixel level assessment were not computed as the ground truth data (i.e. manually delineated polygons) was not accurate at the pixel level. Hence a macro level validation was found to be a better metric for interpreting the results.

CHAPTER 7

CONCLUSION AND FUTURE WORK

In this study a complete ITC delineation framework was proposed using multi-spectral LiDAR data. The framework included three routines: data pre-processing, treetop detection and full crown delineation.

In the data pre-processing phase, the LiDAR intensity data and the LiDAR positional information were merged using a proposed integration strategy. A complete work flow to radiometrically correct the multispectral LiDAR data and co-register it with the LiDAR positional information was outlined and implemented. The three channels were individually processed to remove the effect of ranges from the intensity data. The LiDAR positional information was processed to extract the true canopy dimensions via a CHM.

In the second phase, the pre-processed LiDAR positional data was used to identify the treetops using an improved multi-scale method. The morphology of the LiDAR data was extensively exploited in refining the initial tree localization in the treetop identification phase to improve the quality of segmentation and reduce commission and omission errors. The previously developed multi-scale method was able to account for varying crown sizes in the scene, but a meaningful approach to merge the tops at different scales was not

presented. At smaller scales the original multi-scale method was able to accurately detect crowns of smaller size, but this inevitably yielded a higher commission error in dense tree clusters or for large tree crowns, as multiple false tops were detected due to a smaller scale size. The improved method, developed in this study, was able to accurately integrate the treetops from different scales by extensively exploiting the natural morphology of the tree crown present in the LiDAR CHM. In this study, the topology of the tree crown was modelled by a Gaussian function and treetops at different scales were merged based on residual analysis. The multiple false treetops at smaller scales (originating from upper branches of the tree crown) were merged into a single top at larger scale, hence reducing commission errors. Due to the lack of ground truth information for treetops, only a qualitative analysis was performed to evaluate the results of the proposed multi-scale method. However a quantitative analysis was performed for the final delineated segments derived from treetops detected using the proposed multi-scale method.

In the final stage of ITC delineation, the identified treetops were used as initial approximate locations (i.e. seeds) of the tree crowns in a neutrosophic seeded region growing algorithm. Neutrosophic logic was effectively used, in this study, for the first time, to mitigate the effect of noise in the intensity data by exploiting contextual information around the seed to derive more accurate decision heuristics. The LiDAR positional information was incorporated as a constraint on the morphology of the growing regions. Unlike other region-based and watershed segmentation methods, which were either suited for optical imagery or LiDAR data, the proposed method was illustrated to effectively exploit both data sources and yield accurate results. To provide an independent examination of the

results, reference treetops were used to segment the regions and provide a more relevant comparison with the manually delineated polygons. The results indicated that neutrosophic logic was able to extensively exploit the intensity information to segment the crown boundaries however the segmented regional boundaries were coarse and did not align with the structural boundaries of the tree crowns. The LiDAR positional information was therefore shown to resolve this issue by constraining the growth of the regions beyond the structural boundary of the crown in the CHM. Hence by combining the LiDAR positional and intensity information the boundaries of the segmented regions were refined using a simple yet effective region growing module.

The results of the proposed method were compared with the popular flood fill variant of the Marker Controlled Watershed (MCW) segmentation. The MCW method primarily relied on the assumed topology in the scene, hence it was particularly sensitive to the noise in intensity data. The assumed topology of the watershed method, where the treetop represents the point of highest ‘elevation’ and subsequent points are of lower ‘elevation’ (with the boundary of the crown being the lowest point) were inherently captured in the proposed LiDAR shape constraint, as it was deemed to best describe the morphology of the crown. However a similar assumption about the spectral response was not made as it did not conform to the nature of the intensity information. Hence the proposed method was able to produce higher accuracy metrics than the watershed method by exploiting the natural characteristics of each data source.

Using combined spectral data and LiDAR positional information was able to provide reasonably accurate ITC delineation results. However for individual isolated crowns, in urban areas, the intensity information was best able to isolate the ITCs due to the variation (in spectral domain) between the crown and other cover types. For dense tree clusters (in urban or forest areas), the LiDAR positional information was particularly useful in isolating ITCs from adjacent crowns based on the vertical profile and general morphology of the crown. However due to the high density of the ITCs in the forest area and a high overlap between adjacent crowns, erroneous segmentation results were observed. The results indicated over and under segmentation for dense tree clusters. Certain regions were also completely omitted or over-segmented to a size much larger than the reference polygon. However to provide a complete and accurate picture of the segmentation quality, these outliers were accounted for in the quoted accuracy metrics.

The combination of LiDAR positional information and spectral data shows a great potential for ITC delineation studies. Multispectral LiDAR data provides a good opportunity to examine the benefits of integrating different data sources for ITC delineation purposes. However the intensity information present in the LiDAR data is often low resolution and contaminated with high noise levels. This prevents a meaningful integration of the two different data sources to examine the benefits in the discipline of ITC delineation. In this research, a neutrosophic logic based merging approach was used to mitigate the effect of noise in the intensity data to improve the quality of segmentation. However the quality of the intensity information must be improved for multispectral LiDAR data to be used as a replacement for optical imagery.

In future work, the proposed method can be applied to the combined dataset with CHM derived from LiDAR data and multispectral/hyperspectral data from passive optical imagery. Though issues exist in the co-registration of the two datasets, as outlined in this study, an integrated LiDAR and optical imagery dataset can offer rich spectral and positional information. In this study the CHM was exploited in the treetop detection phase. Though accurate results were obtained, a higher commission error was observed due to the complex upper branch structure in dense deciduous crowns. In future efforts, the LiDAR positional information can be combined with the multispectral data, from optical imagery, to reduce the commission error in treetop identification in dense deciduous crowns.

To further improve the multi-scale analysis proposed in this study, statistical tests can be used during residual analysis. In this study, a Gaussian function was used to model the treetops at different scales. Consequently, residual analysis was used to select the appropriate scale at which the treetop was initialized. Though residual analysis worked well in this study, the method did not consider if the residuals at different scales significantly varied from each other. In future work, the residual analysis can be modified by performing a statistical test to determine if residuals at two different scales are significantly different from each other. Hence treetops at smaller and upper scale can be merged based on statistical test.

In the segmentation results, with initial seeds generated using the proposed multi-scale method, a larger number of segments intersected a common reference polygon. This effect

was primarily attributed to the erroneous treetop detection, where multiple treetops were initialized for a single crown. Hence each treetop was grown, during region growing, to represent a section of the crown, which inevitably contributed towards a higher number of partial matches or complete omissions. Though the results may be significantly improved by reducing the error in the treetop detection phase, a post-segmentation merging process can also be used to improve the segmentation results. By using a measure of spectral variance adjacent regions can be merged together. Conversely in cases of over-segmentation, where certain regions grow much larger than the corresponding reference polygons, splitting strategy can be used to split the region into smaller regions. Though the initial treetop detection remains central to an accurate segmentation, post-segmentation processes can be certainly exploited to increase the overall quality of the results.

In this study, deep learning methods for instance segmentation were not used due to limitations in the training data. However recent architectures have been proposed that circumvent the problem of requiring copious amounts of training data. One such network, based on the encoder-decoder architecture, is known as U-Net. The U-Net architecture, originally proposed for biomedical image segmentation, can be trained on smaller training datasets to segment the crown boundaries. Due to addition of activation maps from earlier layers in the network, fine-grain spatial information can be retrieved to precisely detect object boundaries. Hence in future endeavours, the U-Net architecture can be exploited to further improve ITC delineation.

CHAPTER 8

BIBLIOGRAPHY

Axelsson, P.; DEM generation from laser scanner data using adaptive TIN models. *International Archives of Photogrammetry and Remote Sensing*, 33, 111–118, 2000.

Baartz, M.; Schape, A. Multiresolution Segmentation: an optimization approach for high quality multi-scale image segmentation., 2000.

Baltsavias, E. P. Airborne laser scanning: basic relations and formulas. *ISPRS Journal of photogrammetry and remote sensing*, 54(2-3), 199-214, 1999.

Beucher, S.; Meyer, F.; "Segmentation: The Watershed Transformation. Mathematical Morphology in Image Processing." *Optical Engineering*, 34. 433-481, 1993.

Beucher, S.; Lantuejoul, C.; "Use of watersheds in contour detection." *International Workshop on Image Processing, Realtime Edge and Motion Detection/Estimation*, 12–21, 1979.

Beucher, S.; Serra, J.; Soille, P. Watershed, hierarchical segmentation and waterfall algorithm. Mathematical Morphology and its Applications to Image Processing. *Serra & Soille, Springer, Heidelberg*, 69-76, 1994.

Brandtberg, T.; Walter; F. "Automated delineation of individual tree crowns in high spatial resolution aerial images by multiple-scale analysis." *Machine Vision and Applications*, 11, 64–73, 1998.

Breidenbach, J.; Næsset, E.; Lien, V.; Gobakken, T.; Solberg, S. Prediction of species specific forest inventory attributes using a nonparametric semi-individual tree crown approach based on fused airborne laser scanning and multispectral data, *Remote Sensing of Environment*, 114.4, 911-924, 2010.

Chen, Q.; Baldocchi, D.; Gong, P.; Kelly, M. Isolating individual trees in a savanna woodland using small footprint lidar data. *Photogrammetric Engineering & Remote Sensing*, 72.8, 923-932, 2006.

Culvenor, D. S. TIDA: an algorithm for the delineation of tree crowns in high spatial resolution remotely sensed imagery. *Computers & Geosciences*, 28, 33–44, 2002.

Diaz, F. J.C.; Carter, W.E.; Glennie, C.; Shrestha, R.L.; Pan, Z.; Ekhtari, N.; Singhania, A.; Hauser, D.; Sartori, M. Capability Assessment and Performance Metrics for the Titan Multispectral Mapping Lidar. *Remote Sens*., 8, 936, 2016.

Erikson, M. Species classification of individually segmented tree crowns in high-resolution aerial images using radiometric and morphologic image measures. *Remote Sensing and Environment*, 91.3, 469–477, 2004.

Gougeon, F. A.; Donald G. L. "The individual tree crown approach applied to Ikonos images of a coniferous plantation area. *Photogrammetric Engineering & Remote Sensing.* 72.11, 1287-1297, 2005.

Gougeon, F. A. A crown-following approach to the automatic delineation of individual tree crowns in high spatial resolution aerial images. *Canadian journal of remote sensing* 21.3, 274-284, 1995.

Gong, P.; Sheng, Y.; Biging, G. S. 3D model-based tree measurement from high-resolution aerial imagery. *Photogrammetric Engineering and Remote Sensing*, vol. 68, pp. 1203-1212, 2002.

Hu, B.; J. Li; L. Jing; Judah A. Improving the efficiency and accuracy of individual tree crown delineation from high- 3184 density LiDAR data. *International Journal of Applied Earth Observation and Geoinformation*, 26, pp. 144-155, 2014.

Hyyppä, J.; Mielonen, T.; Hyyppä, H.; Maltamo, M.; Yu, X.; Honkavaara, E.; Kaartinen, H. Using individual tree crown approach for forest volume extraction with aerial images and laser point clouds. *In Proceedings of the International Archives of the Photogrammetry, Remote Sensing and Spatial Information Sciences*, 36 (3/W19), Enschede, The Netherlands, 12–14; pp. 144–149, September 2005.

Jing, L.; Hu, B.; Li, J.; Noland, T. Automated delineation of individual tree crowns from LiDAR data by multi-scale analysis and segmentation. *Photogrammetric Engineering & Remote Sensing*, 78(12), 1275-1284, 2012.

Carter, J.; Schmid, K.; Waters, K.; Betzhold, L.; Hadley, B.; Mataosky, R.; Halleran, J. An introduction to LiDAR technology, data, and applications. *NOAA Coastal Services Center*, 2, 2012.

Johannes B.; Erik N.; Vegard L.; Terje G.; Svein S. Prediction of species specific forest inventory attributes using a nonparametric semi-individual tree crown approach based on fused airborne laser scanning and multispectral data. *Remote Sensing of Environment*, Volume 114, Issue 4, Pages 911-924, 2010.

Judah, A.; B. Hu; Wang, J. An algorithm for boundary adjustment toward multi-scale adaptive segmentation of remotely sensed imagery. *Remote Sensing*, 6, 3583-3610, 2014.

Jutzi, B.; Gross, H. Normalization of LiDAR intensity data based on range and surface incidence angle. *Int. Arch. Photogramm. Remote Sens. Spat. Inf. Sci*, 38, 213-218, 2009.

Kandare, K.; Dalponte, M.; Gianelle, D.; Chan, J.C. "A new procedure for identifying single trees in understory layer using discrete LiDAR data," 2014 IEEE Geoscience and Remote Sensing Symposium, Quebec City, QC, 2014, pp. 1357-1360.

Kwak, D. A.; Lee, W. K.; Lee, J. H.; Biging, G. S.; Gong, P. Detection of individual trees and estimation of tree height using LiDAR data. *Journal of Forest Research*, 12(6), 425-434, 2007.

Koch, B., U.; Heyder W.; Weinacker H. Detection of individual tree crowns in airborne LiDAR data. *Photogrammetric Engineering and Remote Sens.*, vol. 72, pp. 357–363, 2006.

Leckie, D. G.; Gougeon, F. A.; Walsworth, N.; Paradine, D. Stand delineation and composition estimation using semi-automated individual tree crown analysis. *Remote sensing of environment*, 85(3), 355-369, 2003.

Lee, J.; Coomes, D.; Schonlieb, C. B.; Cai, X.; Lellmann, J.; Dalponte, M.; Morecroft, M. A graph cut approach to 3D tree delineation, using integrated airborne LiDAR and hyperspectral imagery. *arXiv preprint arXiv:1701.06715*, 2017.

Lee, D. T.; Schachter, B. J. Two algorithms for constructing a Delaunay triangulation. *International Journal of Computer & Information Sciences*, 9(3), 219-242, 1980.

Li, W.; Guo, Q.; Jakubowski, K.; Marek M.; Kelly, M. A New Method for Segmenting Individual Trees from the Lidar Point Cloud. *Photogrammetric Engineering and Remote Sensing*. 78. 75-84. 10.14358/PERS.78.1.75, 2012.

Li. J., B. Hu, Woods, M. A two-level approach for identification of species importance to the winter habitat of white-tailed deer among coniferous trees in central Ontario forest. *International Journal of Applied Earth Observation and Geoinformation*, 8(4):1487-1497, 2015.

Li, W.; Fu, H.; Yu, L.; Cracknell, A. Deep learning based oil palm tree detection and counting for high-resolution remote sensing images. *Remote Sensing*, 9(1), 22, 2016.

Long, J.; Shelhamer, E.; Darrell, T. Fully convolutional networks for semantic segmentation. *In Proceedings of the IEEE conference on computer vision and pattern recognition* (pp. 3431-3440), 2015.

Meyer, F.; Beucher, S. Morphological segmentation. *Journal of Visual Communication and Image Representation*, 1 (1), 21-46, 1990

Morsy, S.; Shaker, A.; El-Rabbany, A.; LaRocque, P. E. AIRBORNE MULTISPECTRAL LIDAR DATA FOR LAND-COVER CLASSIFICATION AND LAND/WATER MAPPING USING DIFFERENT SPECTRAL INDEXES. *ISPRS Annals of Photogrammetry, Remote Sensing & Spatial Information Sciences*, *3*(3), 2016.

Naveed F.; Hu B. Individual Tree Crown Delineation Using Multi-Wavelength Titan LiDAR Data. *ISPRS Int. Arch. Photogramm. Remote Sens. Spat. Inf. Sci*., XLII-3/W3, 143–148, 2017.

Novotný, J.; Hanuš, J.; Lukeš, P.; Kaplan, V. Individual tree crowns delineation using Local Maxima approach and seeded region growing technique. *In Proceedings of Symposium GIS Ostrava* (pp. 27-39), 2011.

Pouliot, D. A.; King, D. J.; Bell, F. W.; Pitt, D. G. Automated tree crown detection and delineation in high-resolution digital camera imagery of coniferous forest regeneration. *Remote Sensing of Environment*, Volume 82, Issues 2–3, Pages 322-334, 2002.

Pouliot, D. A.; King, D. J.; Pitt, D. G. Development and evaluation of an automated tree detection-delineation algorithm for monitoring regenerating coniferous forests. *Canadian Journal of Forest Research*, vol. 35, pp. 2332-2345, 2005.

Popescu, S. C.; Wynne, R. H.; Nelson, R. F. Measuring individual tree crown diameter with lidar and assessing its influence on estimating forest volume and biomass. *Canadian Journal of Remote Sensing*, vol. 29, pp. 564–577, 2003.

Shan, J.; Cheng, H. D.; Wang, Y. A completely automatic segmentation method for breast ultrasound images using region growing. *Proceedings of the 9th Int. Conference on Computer Vision, Pattern Recognition, & Image Processing*, 2008.

Schardt, M.; Ziegler, M.; Wimmer, A.; Wack, R.; Hyyppae, J. Assessment of forest parameters by means of laser scanning. *International Archives of Photogrammetry Remote Sensing and Spatial Information Sciences*, XXXIV part 3A, pp. 302–309, 2002.

Serra, J.; Soille, P. Mathematical morphology and its applications to signal processing. *Series Computational Imaging and Vision*, 1994.

Serra, J.; and Pierre S. Mathematical morphology and its applications to image processing. *Springer Science & Business Media*, Vol. 2, 2012.

Vincent, L.; Soille, P. Watersheds in digital spaces: an efficient algorithm based on immersion simulations. *IEEE Transactions on Pattern Analysis and Machine Intelligence*, 13 (6), pp. 583-598, 1991.

Vosselman, G., “Slope based filtering of laser altimetry data.” International Archives of Photogrammetry and Remote Sensing, pt. B3, vol. 33, pp. 958–964, 2000.

Wang, L.; Peng, G.; Gregory S. B. Individual tree-crown delineation and treetop detection in high-spatial-resolution aerial imagery. *Photogrammetric Engineering & Remote Sensing* 70.3, 351-357, 2004.

Wehr, A.; Lohr, U. Airborne laser scanning—an introduction and overview. *ISPRS Journal of photogrammetry and remote sensing*, 54(2-3), 68-82, 1999.

Wolf, B.M.; Heipke, C. Automatic extraction and delineation of single trees from remote sensing data. *Machine Vision and Applications* 18 (5), 317–330, 2007.

Xiao, C.; Qin, R.; Huang, X.; Li, J. A STUDY OF USING FULLY CONVOLUTIONAL NETWORK FOR TREETOP DETECTION ON REMOTE SENSING DATA. *ISPRS Annals of Photogrammetry, Remote Sensing & Spatial Information Sciences*, 4(1), 2018.

Yan, W. Y.; Shaker, A. Radiometric correction and normalization of airborne LiDAR intensity data for improving land-cover classification. *IEEE Transactions on Geoscience and Remote Sensing*, 52(12), 7658-7673, 2014.

Yan, W. Y.; Shaker, A. Radiometric normalization of overlapping LiDAR intensity data for reduction of striping noise. *International journal of digital earth*, 9(7), 649-661, 2016.

Yan, W. Y.; Shaker, A. Correction of overlapping multispectral LiDAR intensity data: polynomial approximation of range and angle effects. *The International Archives of Photogrammetry, Remote Sensing and Spatial Information Sciences*, 42, 177, 2017.

Yu, X.; Hyyppä, J.; Kaartinen, H.; Maltamo, M. Automatic detection of harvested trees and determination of forest growth using airborne laser scanning. *Remote Sensing of Environment*, 90(4), 451-462, 2004.

Zhen, Z.; Quackenbush, L. J.; Zhang, L. Trends in Automatic Individual Tree Crown Detection and Delineation-Evolution of LiDAR Data. *Remote Sensing*, 8(4), pp. 333, 2016.

Zhen, Z.; Quackenbush, L. J.; Stehman S. V.; Zhang, L. Agent-based region growing for individual tree crown delineation from airborne laser scanning (ALS) data, *International Journal of Remote Sensing*, 36:7, 2015.

Zhang, W. Individual Tree Crown Delineation Using Combined LiDAR Data and Optical Imagery. MS. Thesis, York University, 2009.

Zhang, J.; Sohn, G. A Markov Random Field Model for Individual Tree Detection from Airborne Laser Scanning Data. *International Archives of the Photogrammetry, Remote Sensing and Spatial Information Sciences - ISPRS Archives*. 38, 2010

Zhao, X.; Guo, Q.; Su,Y.; Xue, B. Improved progressive TIN densification filtering algorithm for airborne LiDAR data in forested areas. *ISPRS Journal of Photogrammetry and Remote Sensing*, vol. 117, pp.79-91, 2016.

Zou, X.; Zhao, G.; Li, J.; Yang, Y.; and Fang, Y. 3D LAND COVER CLASSIFICATION BASED ON MULTISPECTRAL LIDAR POINT CLOUDS, *Int. Arch. Photogramm. Remote Sens. Spatial Inf. Sci*., XLI-B1, 741-747, 2016.